MODELING OF HYBRID ELECTRIC VEHICLE BATTERIES

by

RAMACHANDRA MADDALA, B.E.

A THESIS

IN

ELECTRICAL ENGINEERING

Submitted to the Graduate Faculty
of Texas Tech University in
Partial Fulfillment of
the Requirements for
the Degree of

MASTER OF SCIENCE

IN

ELECTRICAL ENGINEERING

Approved

May, 2003

ACKNOWLEDGEMENTS

I express sincere thanks to Dr. Micheal Parten, my advisor who was involved in the completion of my thesis. My graduate studies would not have been possible without his able teaching and guidance. I would also like to thank Dr. Thomas Krile for being my thesis committee member.

I would also thank all my family members for their encouragement over the years. My thanks to Mr. Kumar Buduri for his support and help during the finishing stage of my thesis.

CONTENTS

ABSTRACT

Battery models are essential in estimating the performance, life and operating characteristics, which are required for hybrid electric vehicle analysis. The battery discharge and charge models are developed and explained in detail. The two models are directly based on the empirical data from literature and manufacturers data sheet. Detail analysis in the development of empirical equations using interpolation and curve fitting methods is provided. Datafit 8.0.32 and TableCurve2D are used to fit the data and Simulink is used in developing the model. Gassing which affects the performance characteristics of batteries is included in the charge model. The overall battery model is assumed to be in a vehicle and tested for a driving cycle to observe the simulation results.

LIST OF TABLES

LIST OF FIGURES

CHAPTER I

INTRODUCTION

At the turn of the century, there is a growing dependence (Fig. 1.1) on imported oil and heightened concern on environment, which led major vehicle manufacturers to sponsor research into advanced transportation technologies. One of theses future developments is the Hybrid Electric Vehicle (HEV) technology. Emissions reductions, while obtaining superior fuel economy, as well as the flexibility of using either petroleum or alternative fuels are the development goals for this progressive technology. As a possible solution to the worldwide interest in environment, the Department of Energy (DOE) is committed to making hybrid electric vehicles commonplace on American highways during the next decade [1].

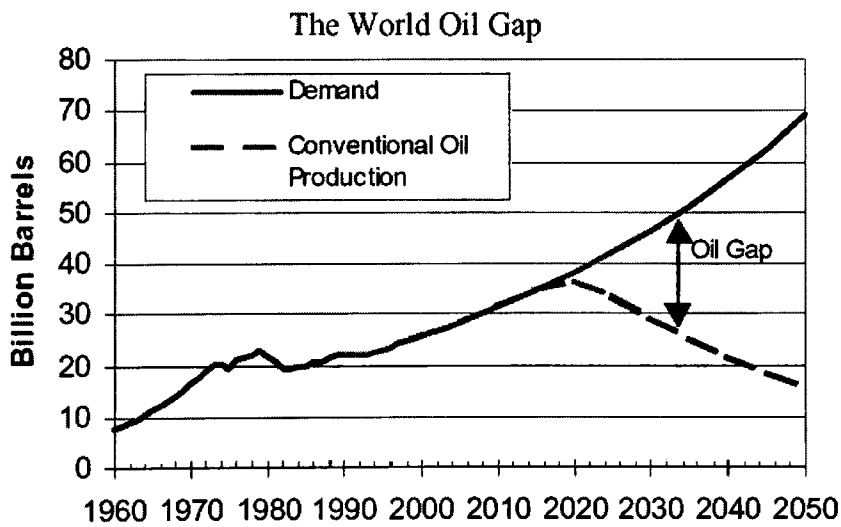

Fig. 1.1 Growing dependence on oil [2]

Hybrid Electric Vehicles (HEVs) combine two or more energy conversion technologies with one or more energy storage technologies. The combination offers extended range with possibility of reducing emissions and fuel consumption.

1.1 Background of Vehicle Configurations

1.1.1 Electric Vehicles

Electric vehicles are propelled by electric motor, whose energy is derived from rechargeable batteries and are much preferred on account of cleanliness, safety and ease of manipulation. The fact that storage batteries must be periodically recharged from some primary electrical source, which reduces the sphere of efficient operation, is one of their main disadvantages [2].

1.1.2 Hybrid Electric Vehicles

A hybrid is a vehicle that uses two or more sources of power. The two sources are electricity from batteries and mechanical power from an internal combustion engine. This combination offers very low emissions of electric vehicles with the power and range of gasoline vehicles. They also offer up to 30 more miles per gallon perform as well or better than any comparable gasoline powered vehicle and never have to be plugged in for recharging [3]. Many configurations are possible for HEVs. There are many ways to combine the engine, motor/generator, and battery. Two basic hybrid configurations are the series and parallel [3].

1.1.2.1 Parallel Hybrid Configuration

An HEV with parallel configuration (Fig. 1.2) has two power paths, so that either the engine or the electric propulsion system or both can be used to turn the wheels. In one approach, the electric only mode can be used for short trips. For longer trips, the power created from an internal combustion would provide power to the vehicle, with the electric motor assisting during high power demand. Such a vehicle reduces weight and provides greater fuel economy [3].

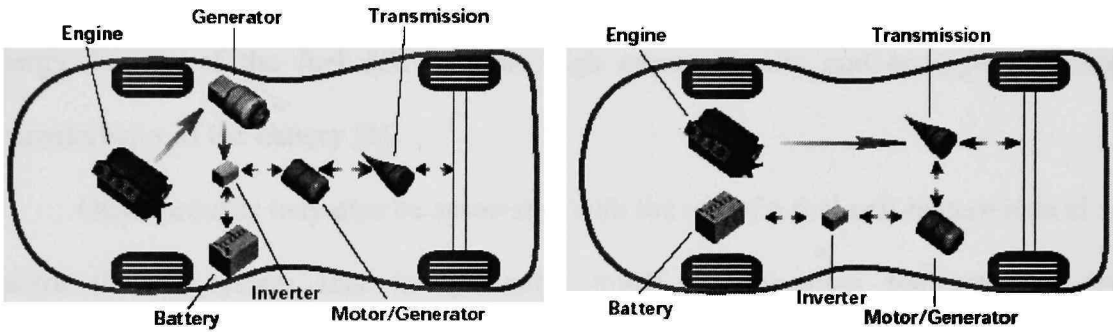

Fig 1.2 Comparison of series and parallel HEV configurations [3]

1.1.2.2 Series Hybrid Configuration

An HEV with series configuration (Fig. 1.2) uses fuel-burning engine and directly drives an alternator to produce electricity. The electricity is stored in the battery pack or sent to the electric motor, which powers the wheels. The vehicle can operate in zero-emission mode completely on electric power from batteries, and the engine turns on to

recharge the batteries. The engine can operate within a narrower and more efficient range of speeds since it is less dependent on the vehicle's changing power demands [3].

1.1.3 Fuel Cell Hybrid Electric Vehicles

Fuel cell-battery hybrid power sources appear to be well suited to overcome both the so-called battery problem (low energy density) and the fuel cell problem (low power density) without having to resort to the addition of an internal combustion engine. The batteries can be recharged by the fuel cells during periods of low power operation. Hybrid operation will therefore permit the most efficient use of the inherently high energy density of the fuel cell and the high power density and energy-interchange characteristics of the battery [4].

Other benefits may also be associated with the use of a fuel cell-battery hybrid, an electric-electric system that is inherently much simpler than the corresponding mechanical-electric hybrid. For example, the battery allows rapid fuel cell start up and protects the fuel cells against cell reversal during this operation. Batteries also have much longer life under the shallow cycling conditions characteristic of hybrids than they do under deep discharge, as occurs in a conventional traction-battery electric vehicle. A fuel cell-battery power plant offers the best of all worlds: good performance, long range, fast refueling and long life.

1.2 Energy Storage Technologies for Hybrid Electric Vehicles

High-power battery technology is being considered for vehicular applications. Nickel/metal hydride (NiMH) batteries currently used in HEVs have been identified to succeed in meeting the high-power requirements. They offer good power capability and their components are recyclable. The main challenges of these batteries are their high cost, the need to control hydrogen loss, and their low cell efficiency [5]. HEV batteries require a higher power-to-energy ratio than electric vehicle batteries.

1.3 Thesis Objective

Texas Tech University is actively involved in developing hybrid electric vehicles for more than a decade. The departments of Electrical Engineering and Mechanical Engineering have focused on developing hybrid electric vehicles with various configurations powered by fuel cell, IC engine and batteries. These batteries power various electrical systems needed in the start up procedure and operation of the vehicle. The batteries used currently in developing HEVs by Texas Tech University are Nickel metal hydride batteries. Nickel metal hydride battery operation is accompanied by the generation of oxygen gas at the nickel electrode. This controls the charge acceptance at high charging rates as well as causes an excessive build up of pressure during charge and overcharge. This problem affects the performance and life of NiMH batteries and raises safety concerns in vehicular applications. It is thus important to understand the capabilities for not only the active material utilization but also the battery conditions resulting from the oxygen reactions in NiMH batteries. ADVISOR 2002 is a simulation

tool used to observe the performance of batteries of various vehicles. Unfortunately, this does not give the complete picture of various issues related with the battery performance. This thesis is about the modeling of Nickel metal hydride (NiMH) batteries. The goal of this work is, therefore, to (1) incorporate charge and discharge voltage characteristics of the NiMH battery by developing simulink-macro models of the charge and discharge behavior in driving conditions and (2) to analyze the effects of oxygen reactions on the battery performance specifically on the charge acceptance and cell pressure build up. Using curve fitting and interpolation techniques various relations are developed using charge and discharge data. The model is simulated for a driving cycle and the performance characteristics; state of charge, voltage, and charge efficiency and battery pressure are observed.

1.4 Organization

The organization of the remainder of the thesis is as follows:

Chapter 2 presents a review of the previous work in battery modeling. Various ADVISOR models, Spice models, electrochemical and equivalent circuit battery models are discussed. Chapter 3 describes the battery macro model developed. Relevant equations, data fits and simulink models are described in detail. Chapter 4 deals with the analysis, simulation results and model validation. Chapter 5 summarizes the contributions of the thesis and discusses avenues for future work in the areas of battery modeling for HEV simulations.

CHAPTER II

REVIEW OF PREVIOUS WORK

This chapter contains a number of battery models used for Electric Vehicles and Battery Energy Storage System applications. While extensive research has been carried out to develop new types of batteries and converters to convert the batteries output to useful work, very little work has been done in modeling the battery itself. There are many factors that affect batteries and few mathematical models exist to predict the performance of batteries [6].

Although batteries act like simple electrical energy storage devices, they actually undergo electrochemical processes that make them difficult to understand and model. Thus, the behavior of a battery is a nonlinear function of a various parameters [7]. The most common battery models include: ADVISOR models, Spice macro models, electrochemical models and equivalent circuit models.

2.1 ADVISOR Models

ADVISOR [7] is a simulation tool for use with Matlab and Simulink. ADVISOR has four different battery models. The RC model (resistive-capacitive) includes transient effects in the battery. The Rint model (internal resistance) characterizes the battery with a voltage source and internal resistance developed by Idaho National Engineering Laboratory to model flooded lead-acid batteries. The third model is a Fundamental Lead Acid Model developed at Brigham Young University for National Renewable Energy

Laboratory (NREL). The fourth model is a neural network model of a lead acid battery developed at Colorado University for NREL [7]. Among the models mentioned, none of them give a clear picture of the NiMH battery except the Rint battery model. The Rint model is a basic model with a voltage source and internal resistance, which uses limited data and does not incorporate all the characteristics of the batteries.

2.2 Spice Models

A Microsim application note provides a SPICE model, which simulates the discharge behaviour of nickel metal hydride (NiMH), nickel-cadmium (NiCd), alkaline and lead-acid batteries [8]. The model is shown in Fig. 2.1. A look-up table of the state of

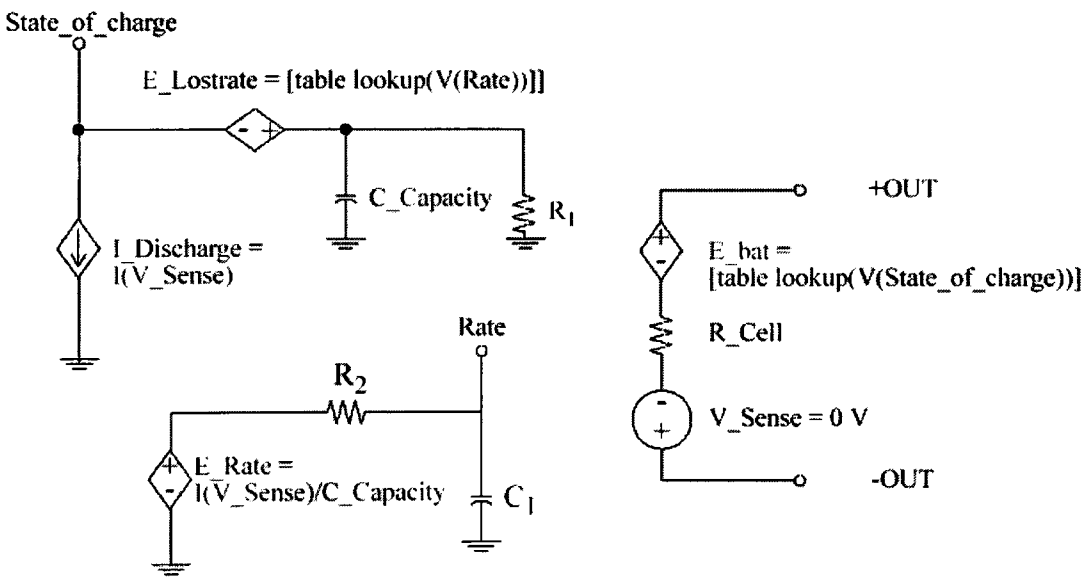

Fig. 2.1 SPICE basic battery model [9]

charge determines the output voltage of the battery. The state of charge is determined by the charge remaining on the capacitor C_Capacity and the discharge rate. The elements R2 and C1 model the delay of the battery in responding to a changing load [9]. However,

the SPICE model does not include many of the NiMH parameters that are important to the safe operation of the batteries.

2.3 Electrochemical Models

Electrochemical models are based solely on electrochemistry and ignore thermodynamic and quantum effects. These models can predict energy storage but are unable to model the time rate of change of voltage under load nor do they include temperature effects [10]. Two basic electrochemical models are described below.

2.3.1. Peukert Equation

In batteries, for higher discharge current, I in amps, there is generally less charge, Q in amp-hours, available. Peukert's equation quantifies this effect [10].

$$Ah = Coeff \times I^{1-n} \qquad \text{---------- 2.1}$$

where

I - is current, in amps,

Ah - is battery capacity, in Amp-hours,

Coeff - constant Peukert coeff,

1-n - Peukert exponent where n is in the range of 1.3 and 1.4 for lead acid batteries.

2.3.2. Shepherd Model Equation

The Shepherd model, perhaps the most often used battery model for HEV analysis, describes the electrochemical behavior of the battery in terms of voltage and

current. It is used in conjunction with the Peukert's equation to obtain battery voltage and state of charge for given load variations [10].

$$E_T = E_0 - R_I I - \frac{K_I}{1-f} \qquad \text{---------- 2.2}$$

where,

E_T battery terminal voltage in volts

E_O - open circuit voltage of a battery when fully charged in volts

R_I - internal resistance of the battery in ohms

K_I - polarization resistance in ohms

Q - Battery capacity in ampere-hour

I - instantaneous current in amps

f = $\int \frac{I}{Q_o} dt$ accumulated ampere-hours divided by full battery capacity.

The fractional state of charge is then found through Peukert's equation.

2.4 Equivalent Circuit Battery Models

Engineers have developed many equivalent circuit models for batteries. Three of the basic models are discussed below.

2.4.1 Simple Battery Model

Fig. 2.2 shows the simple battery model with open-circuit voltage, E_O, and a constant equivalent internal series resistance, ESR. The model does not take into account

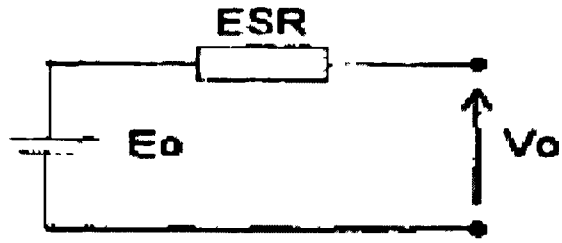

Fig. 2.2 Simple battery model [6]

the varying characteristic of the internal impedance of the battery with the varying state of charge [6]. Such models are applicable in some circuit simulations where the energy drawn out of the battery is assumed to be unlimited or where the state of charge is of little importance. This model is not appropriate for electric vehicle applications.

2.4.2 Thevenin Battery Model

Thevenin battery model consists of an ideal no-load battery voltage (E_O), internal resistance (R), capacitance (C_o) and overvoltage resistance (R_o). C_o represents the capacitance of the parallel plates and R_o represents the non-linear resistance contributed

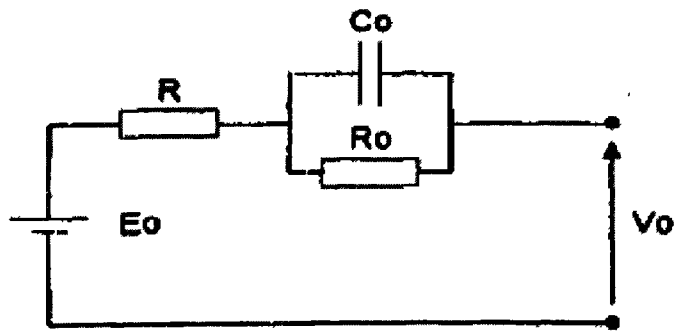

Fig. 2.3 Thevenin battery model [6]

by contact resistance of the plate to electrolyte. All elements in the model are assumed to be constant. In reality, all the elements are functions of battery conditions, which is necessary for the vehicular applications [6].

2.4.3 Improved Battery Model

H.L.Chan and D.Sutanto [6] developed a battery model believed to meet all the requirements compared to Thevenin and the simple battery model. It considers the non-linear battery characteristics both during charging and discharging as well as their dependence on the state of charge of the battery. The characteristic elements shown in Fig. 2.4 include: Self discharge resistance (R_P), which is a function of the open circuit voltage; Charge (R_C) and discharge resistance (R_D) which are associated with the electrolyte, plates and fluid resistance which are different in charging and discharging; Overcharge (R_{CO}) and over discharge resistance (R_{DO}) which increase significantly due to electrolyte diffusion; Battery capacity (C_B) which behaves as a storage capacitor and is

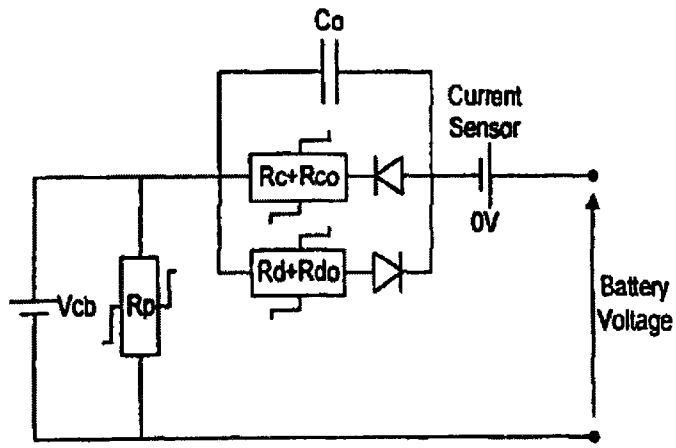

Fig. 2.4 Improved battery model [6]

modeled as a voltage source in SPICE which is a function of state of charge. Since all the elements vary with the open circuit voltage this method provides a relatively better model compared to the previous models.

The main performance characteristics, which need to be incorporated in developing a battery model, include: charge characteristics, specifically the temperature rise (thermal runaway behaviour) and pressure rise in the cells. A majority of the battery models discussed previously are unable to model the rate of change of temperature, pressure and voltage with charge input. The simulink macro model developed in this thesis considers these specific issues during charge and overcharges and was tested for various driving cycles. Chapter III deals with the nickel-metal hydride charge and discharge model.

CHAPTER III

BATTERY MODEL

3.1 Introduction to Battery Modeling

Suitable battery models are indispensable in the design and development of battery operated electrical and electronic systems. This enables simulation of the behavior of the electrical and electronic components in connection with the energy supply system. Simulation models can be developed to some degree from basic physical relationships or directly from empirical data. The most common approach is to used basic physical models when possible and empirical relationship to improve the models performance. However, in some cases, the basic physical relationships are at the microscopic level where the application of the model is at the macroscopic level. In any case, the model must fit actual data. The data used in this thesis is from a number of sources [11, 12, 13]. Using this data, various relations are developed using interpolation and curve fitting techniques.

3.2 Charge Model of NiMH Battery

Nickel metal hydride operation is accompanied by the generation of oxygen gas at the nickel electrode. This controls the charge acceptance at high charging rates as well as causes an excessive build up of pressure during charge and overcharge. This problem affects the performance and life of NiMH batteries and raises safety concerns in vehicular applications. It is thus important to understand the capabilities for not only the active

material utilization but also the battery conditions resulting from the oxygen reactions in NiMH batteries. The mathematical charge model developed in this chapter explores the effects of oxygen reactions on the cell performance during charge and overcharge.

Charging is the process of replacing energy that has been discharged from the battery. The most common charging method for the nickel-metal hydride battery is a constant current charge. The voltage of an NiMH cell during charge depends on a number of conditions. The battery model treats the battery as a store of energy, which incorporates the charging curves for voltage, temperature and pressure vs. charge input.

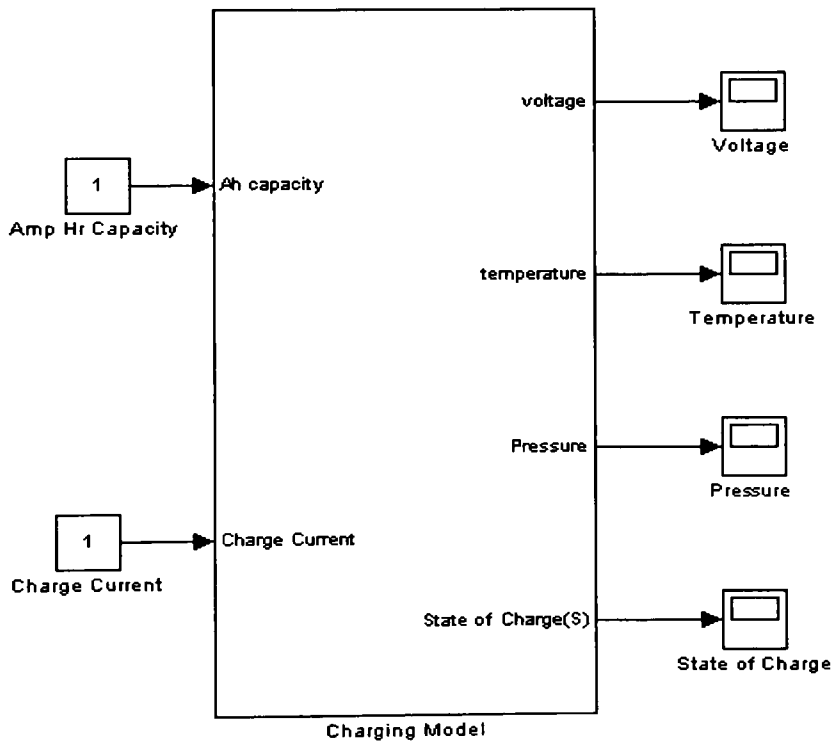

Fig. 3.1 Top-level simulink charge model

Charge input is a function of charge rate and state of charge. The accumulation of the charge input leads to a pressure rise in the battery. Data for a single cell is used to derive several relationships for state of charge, charge acceptance efficiency, voltage and pressure.

The system includes a charge input block, a voltage block, temperature block and a pressure block. Fig. 3.1 shows the top-level simulink model of the NiMH cell with capacity and charge current as the inputs. The outputs of the model are voltage, temperature, charge efficiency, pressure and state of charge.

3.2.1 Modeling the State of Charge Block

The battery model uses a measure of charge added to the battery, the number of Ah, to bring the battery to its completely charged state. Every time step, the "Ah_U" variable is updated according to the relation [14] in Eq. 3.1

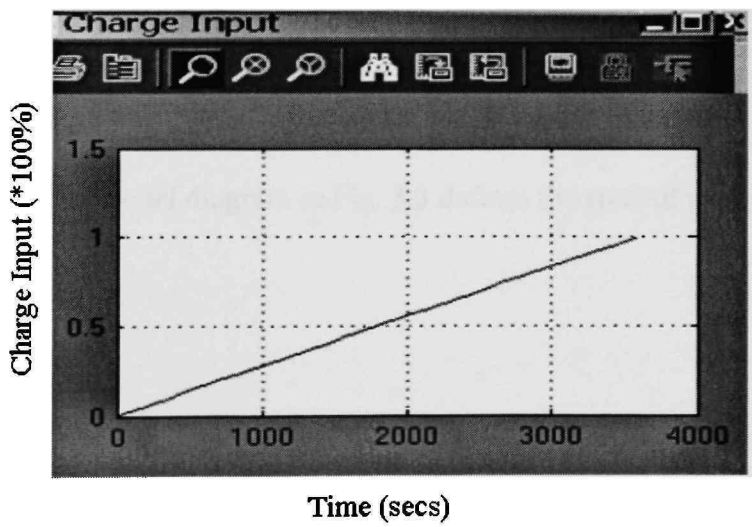

Fig. 3.2 Input amp hrs updated with the simulation time

$$Ah_U = \int(\frac{I_C}{3600})dt, \qquad \text{---------- 3.1}$$

where

Ah_U – is the number of Amp hrs that has been added to the battery during the charging time as shown in Fig. 3.2 (subscript 'u' refers to update)

I_C - is the constant charge current in amps (subscript 'C' used to refer to charge)

t - time in secs.

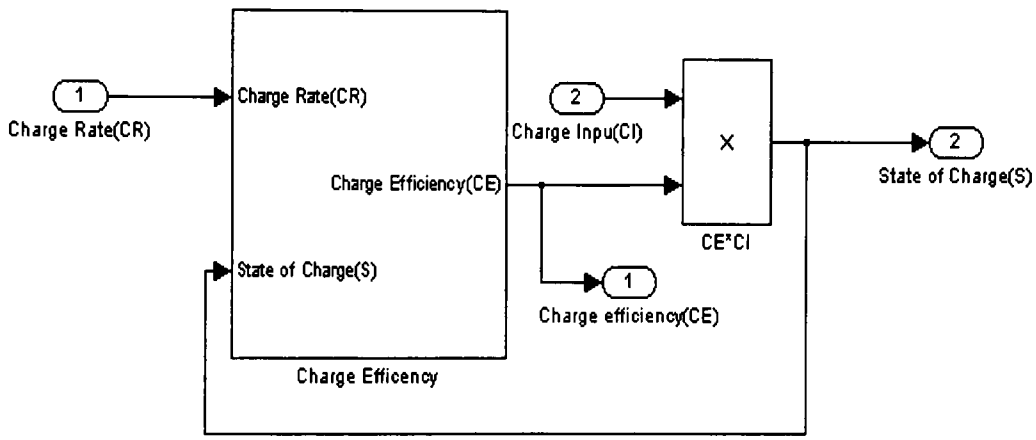

Fig. 3.3 State of charge model

The subsystem in the model diagram in Fig. 3.3 defines the state of charge as [11]

$$S = CE \times C_I, \qquad \text{---------- 3.2}$$

where

S- is the state of charge

CE - is the charge acceptance efficiency

C_I - is the charge input or percentage input of nominal cell capacity given as [15]

$$C_I = \frac{1}{C_P}\int \frac{I_C}{3600} dt \qquad \text{---------- 3.3}$$

C_P - amp hr capacity

I_C - is the charge current.

In order to model the state of charge, an empirical equation is developed for the charge acceptance efficiency parameter or charge efficiency 'CE'. This charge efficiency is a function of state of charge 'S', which is a feedback from the output as shown in Fig. 3.3.

3.2.1.1 Modeling the Charge Efficiency

Charge efficiency is modeled by an empirical equation using the data shown in Fig. 3.4 [11]. There is some function for charge efficiency $CE = f(S, C_R)$ that passes through these data points, where

S - State of charge

C_R – Charge rate.

The state of charge (S) on the x-axis ranges from 0-100% and the charge efficiency (CE) on y-axis varies from 0-100%. The different curves correspond to the charge rate (C_R) that varies form 0.33C to 6C. For every C_R there is a data for state of charge and data for output charge efficiency as shown in Fig. 3.4. With interpolation this function can be approximated such that the functional values between the original data set values can be estimated. Hence the method of interpolation in this case is found by observing the variation of charge efficiency with charge rate at a specified state of charge. For example at 70% state of charge, this variation of charge efficiency is

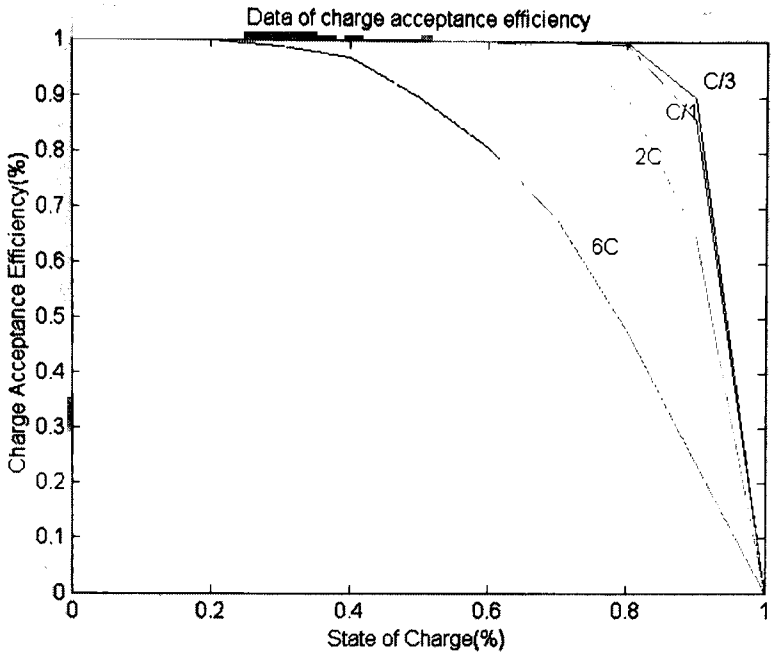

Fig. 3.4 Data for the charge efficiency

observed at the four different charge rates C/3, C/1,2C and 6C and Datafit 8.0 [15] is used to find the best-fit as shown in Fig. 3.5. Datafit has pre-defined models which use non-linear regression to determine the best-fit parameters for a model by minimizing a chosen merit function. The process starts with some initial estimates and incorporates algorithms to improve the estimates iteratively. The new estimates then become a starting point for the next iteration. These iterations continue until the merit function effectively stops decreasing. Although many kinds of models fit the data, it's necessary to observe the behavior of the data points (e.g., exponential, Guassian, etc.) and run the simulation for that model which gives the best fit and minimum error. However, in some cases, when the user-defined function fails to result in a proper fit, the data is run on built-in model equations present in software and the one with minimum error is considered to be the best fit, which happened in most cases throughout this chapter.

As an example the relation between charge efficiency and charge rate is obtained using this software. The coefficients are generated using non-linear regression from the data which gives minimum error. The minimum and maximum residual errors are -6.42331×10^{-5} and 9.261×10^{-5} . The empirical equation is given as

$$CE = 1+0.006378C_R^2 - 0.00623C_R^{2.5}, \qquad \text{----------3.4}$$

where

CE - is the charge acceptance efficiency

C_R – is the charge rate.

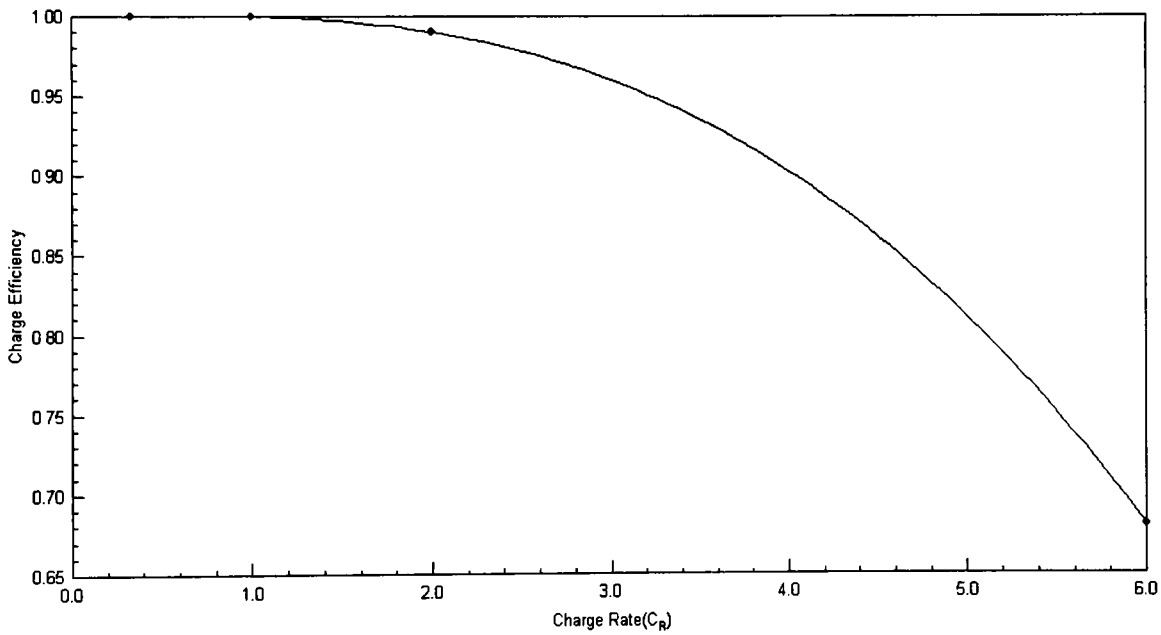

Fig. 3.5 Curve fit for variation of charge acceptance efficiency with charge rate

With this variation of charge efficiency with charge rate, a general form of the equation is used as a method of interpolation to model the charge efficiency block.

The interpolating equation is of the form

$$CE = a + bC_R^2 + cC_R^{2.5}$$ ----------3.5

that passes through the (C_R, CE) support points ($0.33,CE_{0.33}$), ($2,CE_2$) and ($6,CE_6$),

where

$CE_{0.33}$, CE_2 and CE_6 - are charge efficiencies at 0.33C, 2C and 6C charge rates.

Using C_R =0.33C, 2C and 6C in Eq. 3.5 gives a system of three equations

$$CE_{0.33} = a + 0.11b + 5.11c$$ ----------3.5a

$$CE_2 = a + 4b + 5.66c$$ ----------3.5b

$$CE_6 = a + 36b + 88.19c.$$ ----------3.5c

Solving Eq. 3.5(a-c) for the three coefficients 'a', 'b' and 'c' gives

$$a = 0.97CE_{0.33} - 0.09CE_2$$ ----------3.6a

$$b = -0.58CE_{0.33} + 0.62CE_2 - 0.04CE_6$$ ----------3.6b

$$c = 32CE_{0.33} - 35.8CE_2 + 3.89CE_6.$$ ----------3.6c

Substituting the parameters 'a', 'b' and 'c' of Eq. 3.6(a-c) into Eq. 3.5 gives the charge efficiency as

$$CE = (0.97CE_{0.33} - 0.09CE_2) + (-0.58CE_{0.33} + 0.6CE_2 - 0.04CE_6)C_R^2 + (32CE_{0.33} - 35.8CE_2 + 3.89CE_6)C_R^{2.5}$$

----------3.7

where

$$CE_{0.33} = -248S^8 + 834.5S^7 - 1150S^6 + 834.15S^5 - 340.27S^4 + 76.93S^3 - 8.74S^2 + 0.38S + 1$$

----------3.8a

$$CE_{0.2} = \frac{0.66S^2 - 1.66S + 1}{0.18S^3 + 0.48S^2 - 1.61S + 1}$$ ----------3.8b

$$CE_6 = 1.08 - 1.073S^3 - 0.084e^{-S}, \qquad \text{----------3.8c}$$

where

S – is the state of charge.

The curve fitting used to develop Eq. 3.8(a-c) was not from a single program. This is due to the complexity of the data. For example, Eq. 3.8a is generated from the basic fitting tools in Matlab using the polynomial fitting method shown in Fig. 3.6. The residual plot, as shown in Fig. 3.6, justifies the chosen fit with a norm residual of 0.0021515. However, a different approach is used in developing Eq. 3.8b for the charge efficiency at 2C rate. The polynomial fit produced minimum and maximum errors of -0.42 and 0.13, which are considered to be high. TableCurve 2D [16] is a curve fit software package that has a built-in fitting option which processes the data to high precision rational and chebyshev polynomials. As an example, a rational function was chosen to fit this data, which resulted in minimum and maximum residual errors of 0.000079682 and 0.00751126 (Fig. 3.8), justifying the chosen fit as shown in Fig. 3.7. Similarly, the data for CE_6 appears to be a decreasing negative exponential curve, as shown in Fig. 3.9, and hence, a curve fit of the form in Eq. 3.8c is chosen to fit the data using Datafit 8.0. Fig. 3.10 shows the residual error of Fig. 3.9. The minimum and maximum residuals are -0.0258493 and 0.021713.

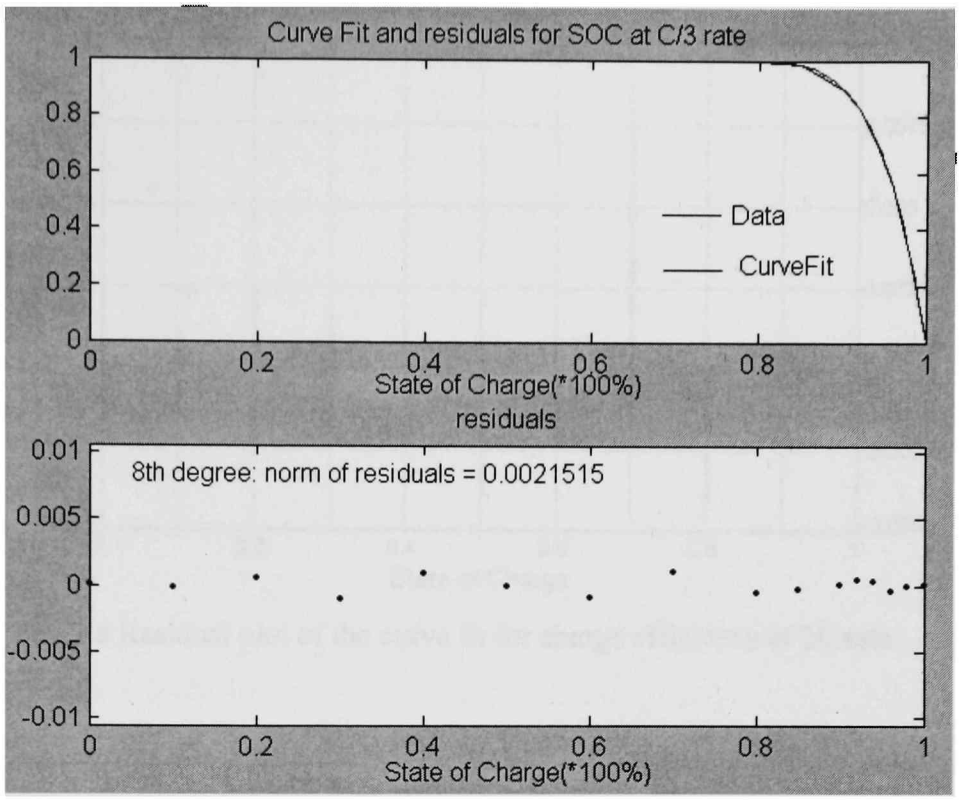

Fig. 3.6 Curve fit and residuals for the charge efficiency at C/3 rate.

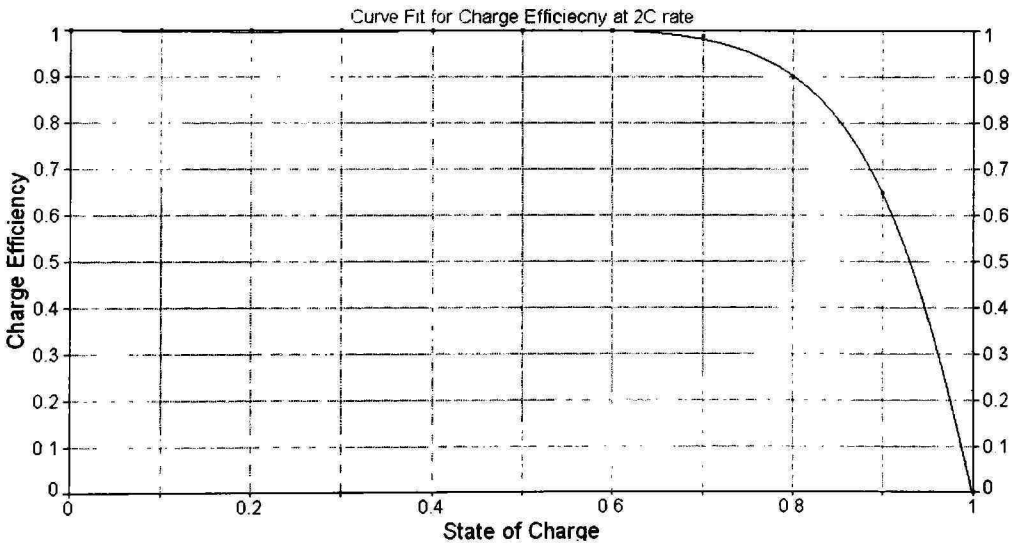

Fig. 3.7 Curve fit for charge efficiency at 2C charge rate

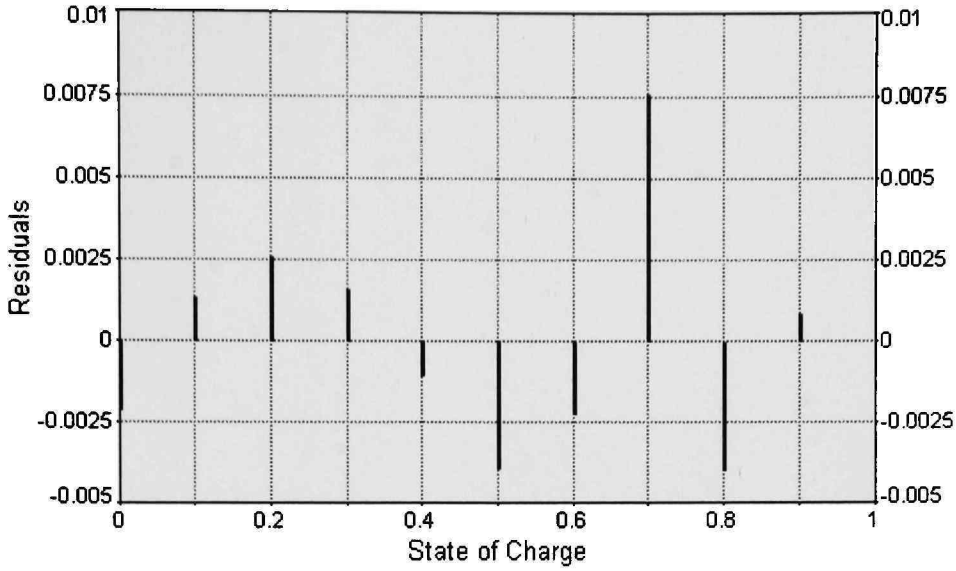

Fig. 3.8 Residual plot of the curve fit for charge efficiency at 2C rate

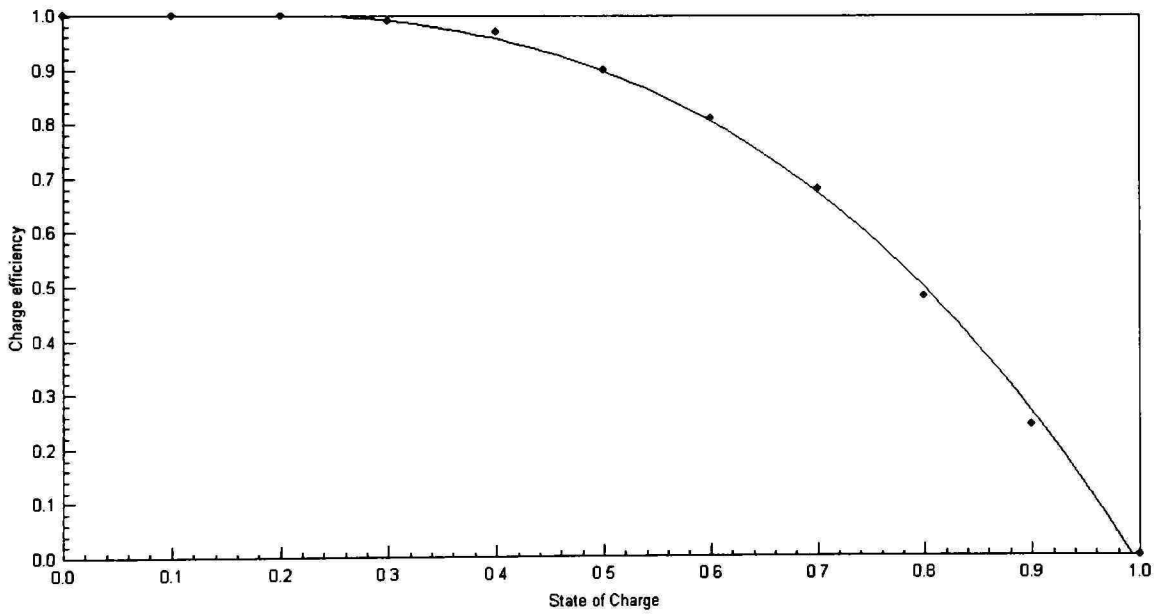

Fig. 3.9 Charge efficiency fit at 6C charge rate

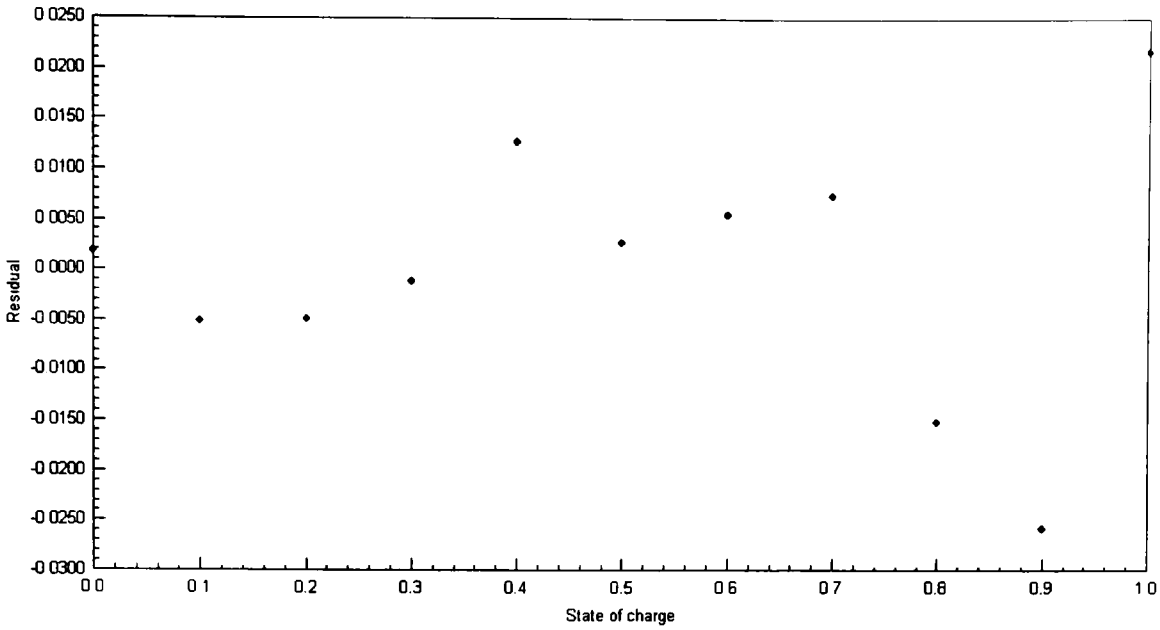

Fig. 3.10 Residuals for charge efficiency at 6C charge rate

Fig. 3.11 is the simulink model, which models Eq. 3.7 with state of charge and charge rate as the inputs and charge acceptance efficiency as the output. The functional blocks a, b and c contains the expressions shown in Eq. 3.7(a-c). Various functional blocks contain the expressions shown in Eq. 3.5(a-c) and Eq. 3.6(a-c).

This charge efficiency block is designed to describe how the oxygen generation during charge reduces the state of charge at higher charging rates. It is obvious that the charge efficiency is strongly dependent on the cell state of charge. When the cell state of charge exceeds 80% the charge acceptance efficiency starts degrading significantly for all charge rates [11].

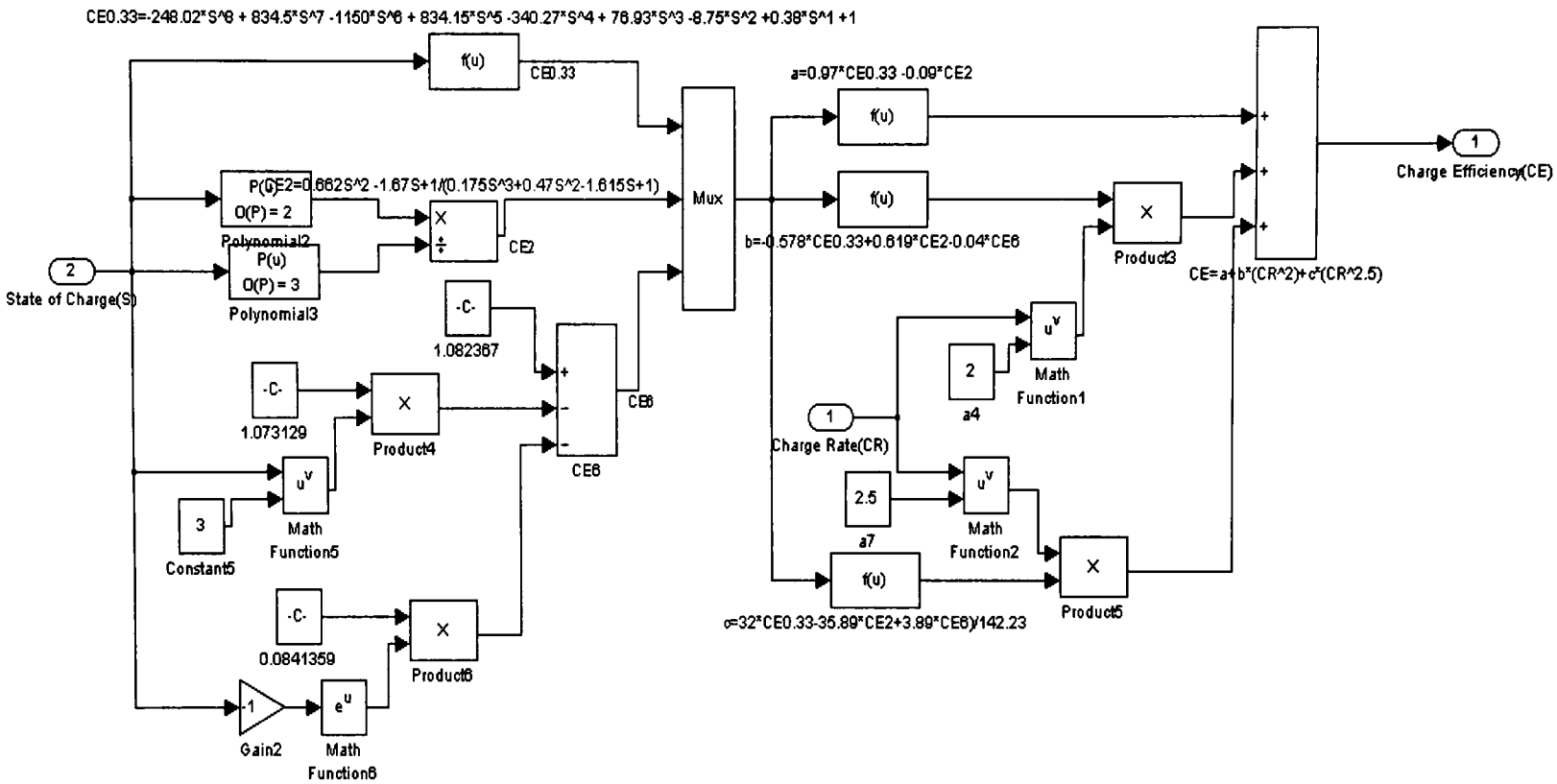

Fig. 3.11 Simulink model of charge efficiency

Having derived the relation for the charge acceptance efficiency CE, the state of charge of the cell used is given by

$$S = CE \times \left(\frac{1}{C_P} \int \frac{I_C}{3600} dt \right), \qquad \text{---------- (3.2)}$$

where

C_P - Amp-hr capacity of the battery

I_C - charge current and

CE - is the charge acceptance efficiency (Eq.3.7)

3.2.2 Modeling the Voltage Block

This block models the voltage profiles at different charge rates. Charge input and charge rate are the inputs to the block and the output is battery voltage. The data used to model this block is shown in Fig. 3.12. The method of interpolation used to determine the voltage for various C_R values is found by observing the variation of voltage with charge rate at specified charge input. At 100% of charge input, this variation of voltage is observed at the four different charge rates C/3, C/1,2C and 6C and Datafit is used to find the proper fit shown Fig. 3.13. The coefficients are software generated from the data which gives minimum residual error. The minimum and maximum residual errors are -6.42331×10^{-5} and 9.261×10^{-5} . The empirical equation is given as

$$V = 1.626157 + 0.031255(\log(C_R))^2 - \frac{0.1261}{\sqrt{C_R}} \qquad \text{----------3.9}$$

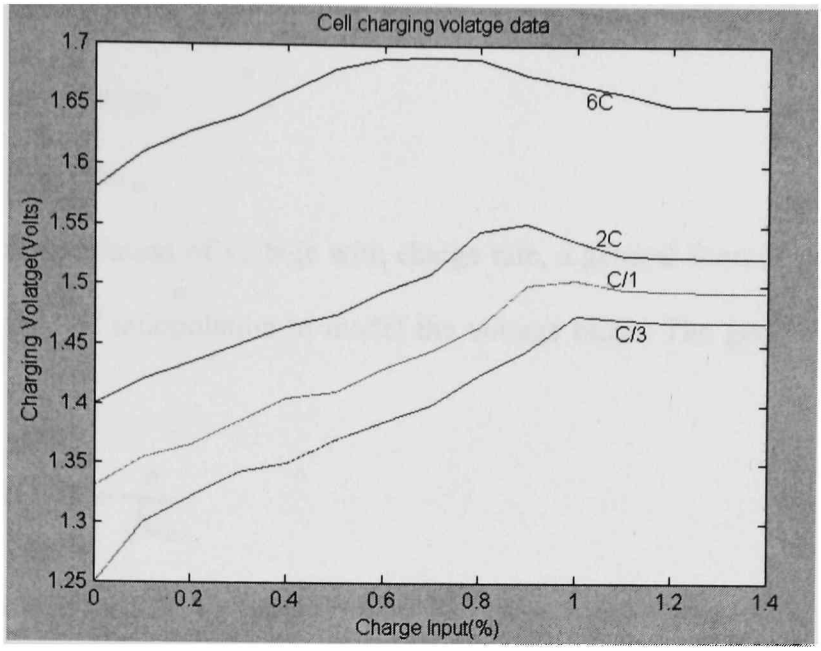

Fig. 3.12 Data for voltage during charging at various charge rates [11]

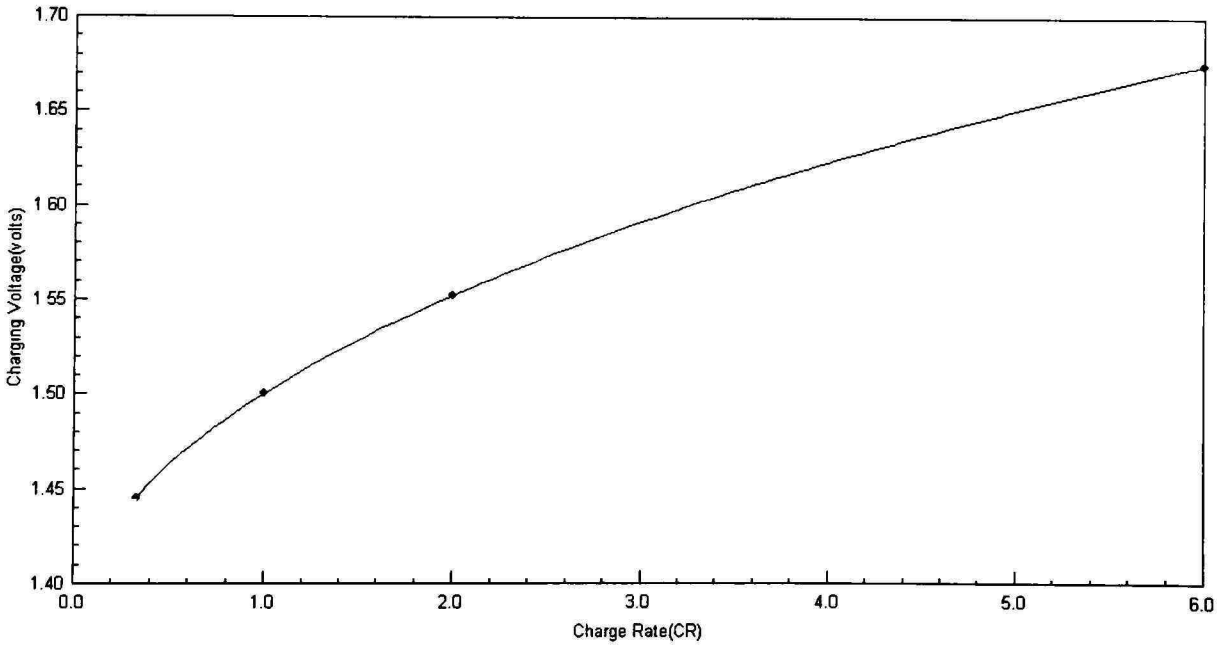

Fig. 3.13 Variation of voltage with charge rate

where

V – is the battery voltage

C_R - is the charge rate.

With this variation of voltage with charge rate, a general form of the equation is used as a method of interpolation to model the voltage block. The general form of this equation is

$$V = a + b(\log(C_R))^2 + \frac{c}{\sqrt{C_R}} \qquad \text{----------3.10}$$

that passes through the (C_R, V) support points ($0.33,V_{0.33}$), ($2,V_2$) and ($6,V_6$)

where,

$V_{0.33}$ and V_2 and V_6 – are fit equations for voltages at C_R=0.33C, 2C and 6C rates.

Using C_R =0.33C, 2C and 6C in Eq. 3.10 gives a system of three equations as

$$V_{0.33} = a + 0.232b + 1.74c \qquad \text{----------3.10a}$$

$$V_2 = a + 0.09b + 0.707c \qquad \text{----------3.10b}$$

$$V_6 = a + 0.606b + 0.408c \ . \qquad \text{----------3.10c}$$

Solving Eq. 3.10(a-c) for the three coefficients 'a', 'b' and 'c' gives

$$a = -0.6806V_{0.33} + 1.6687V_2 + 0.013V_6 \qquad \text{----------3.11a}$$

$$b = 0.5205V_{0.33} - 2.32V_2 + 1.798V_6 \qquad \text{----------3.11b}$$

$$c = 0.897V_{0.33} - 0.65103V_2 - 0.246V_6 \ . \qquad \text{----------3.11c}$$

Substituting the parameters 'a', 'b' and 'c' of Eq. 3.11(a-c) into Eq. 3.10 gives the expression for voltage as

$$V = (-0.6806V_{0.33} + 1.6687V_2 + 0.013V_6) + \left[(0.5205V_{0.33} - 2.32V_2 + 1.798V_6)(\log(C_R))^2\right] + \frac{0.897V_{0.33} - 0.65103V_2 - 0.246V_6}{\sqrt{C_R}}$$

----------3.12

where

$V_{0.33}$, V_2 and V_6 - are fit equations for the voltage at C_R=0.33, 2 and 6 which are functions of charge input C_I given by

$$V_{0.33} = -6.15C_I^8 + 35.2C_I^7 - 81.49C_I^6 + 98.3C_I^5 - 66.8C_I^4 + 26.15C_I^3 - 5.89C_I^2 + 0.89C_I + 1.25$$

----------3.13a

$$V_2 = \frac{2.354C_I^3 - 2.13C_I^2 - 1.42C_I + 1.4}{1.475C_I^3 - 1.171C_I^2 - 1.171C_I + 1}$$

----------3.13b

$$V_6 = -0.69C_I^8 + 5.38C_I^7 - 17.22C_I^6 + 28.9C_I^5 - 26.85C_I^4 + 13.4C_I^3 - 3.355C_I^2 + 0.535C_I^1 + 1.58 .$$

----------3.13c

$V_{0.33}$ and V_6 are the eighth degree polynomial fits shown in Eq. 3.13a and Eq. 3.13c. The norm residuals of both the fits are 0.0011416 and 0.00569250 indicating a suitable fit. However, polyfit of V_2 resulted in an improper fit with minimum and maximum residual errors of -0.112 and 0.17 which is considered inappropriate. Data for V_2 was subjected to Table Curve 2D rational functions and Eq. 3.13b was chosen with minimum residual error of -0.0002674 and the maximum residual error of 0.00355. The generated coefficients are plugged in and compared in Matlab for accuracy. Eq. 3.12 is modeled in simulink as shown in Fig. 3.15. The fit equations of 3.13 (a-c) are represented as the functional blocks in the simulink model, which are referenced with the equations. The inputs to the model are the charge input and the charge rate and the output is voltage.

This block is modeled by the empirical equation 3.12 which incorporates the voltage characteristics between C/3 and 6C charge rates.

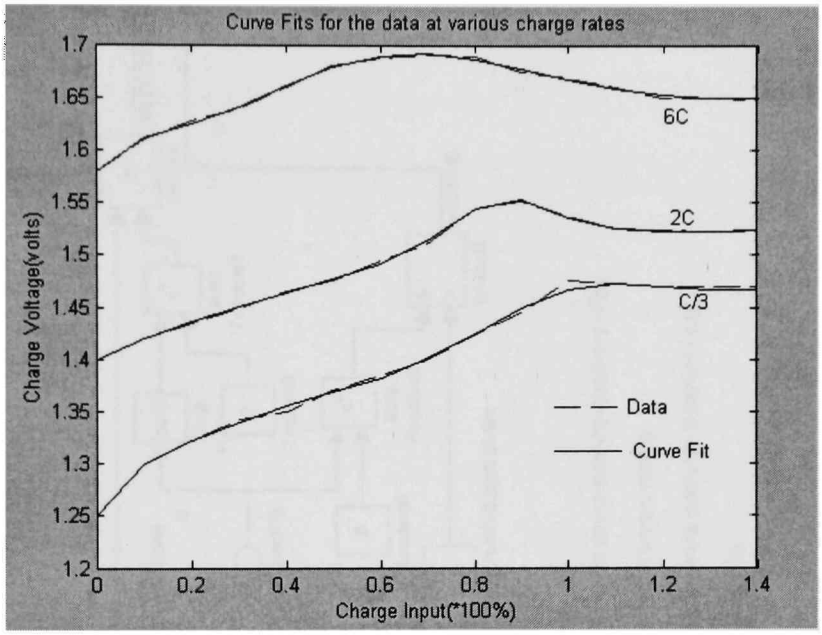

Fig. 3.14 Curve fits for the voltage data [11]

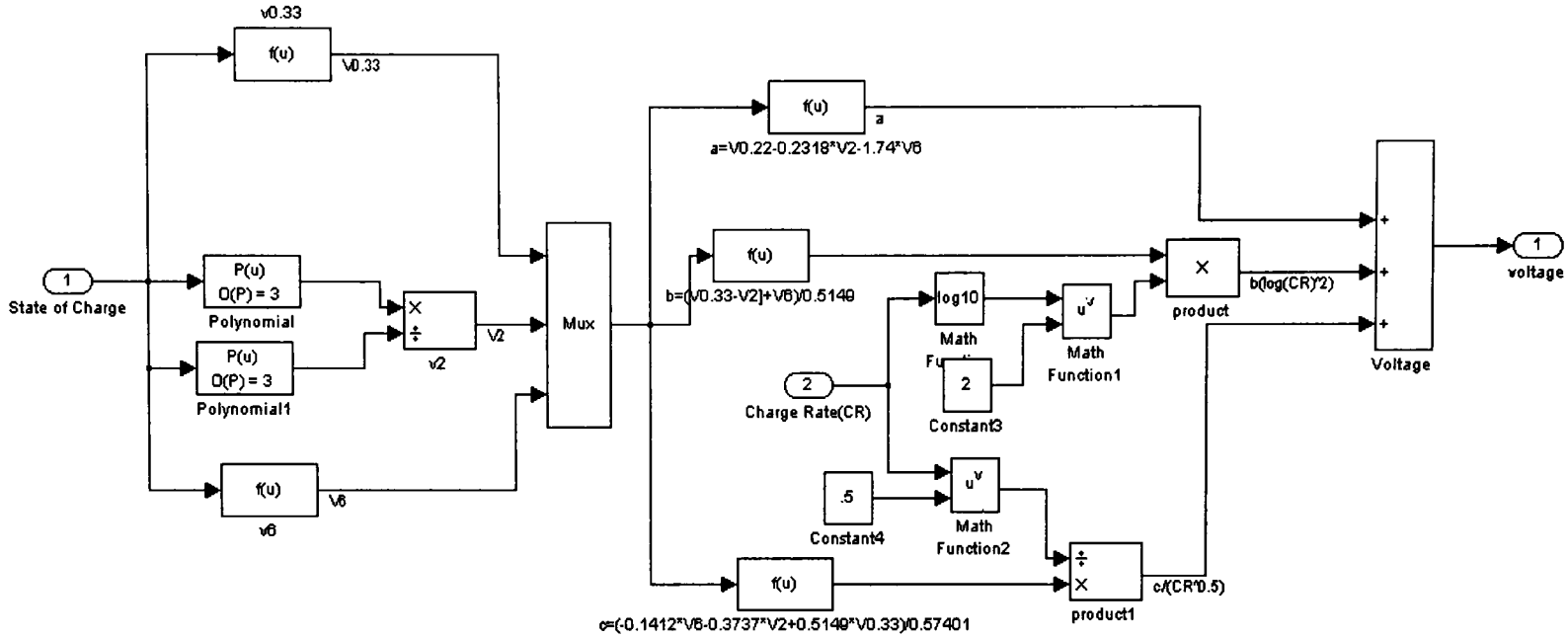

v0.33=-6.15*CI^6 + 35.2*CI^7 -81.49*CI^6 + 98.3*CI^5 -66.8*CI^4 + 26.15*u^3 -5.89*u^2 +0.893*u^1 +1.25

v2=2.35CI^3-2.13CI^2-1.42CI+1.4/([1.476CI^3-1.171CI^2-1.17CI+1)

v6=-0.68*u^8 + 5.38*u^7-17.222*u^6 + 28.9*u^5 -26.86*u^4 + 13.4*u^3 -3.36*u^2 + 0.536*u^1 +1.58

Voltage=a+b*log((CR^2))+c/(CR^0.5)

Fig. 3.15 Simulink model of voltage block

3.2.3 Modeling the Temperature Block

This block models the temperature profiles. The inputs to this block are charge input and charge rate. The data [12] used to model this block is shown in Fig. 3.16. The data is chosen at two intervals at 0.1C and 1C charge rates. Using interpolation techniques, the functional values of cell temperature rise in between these intervals can

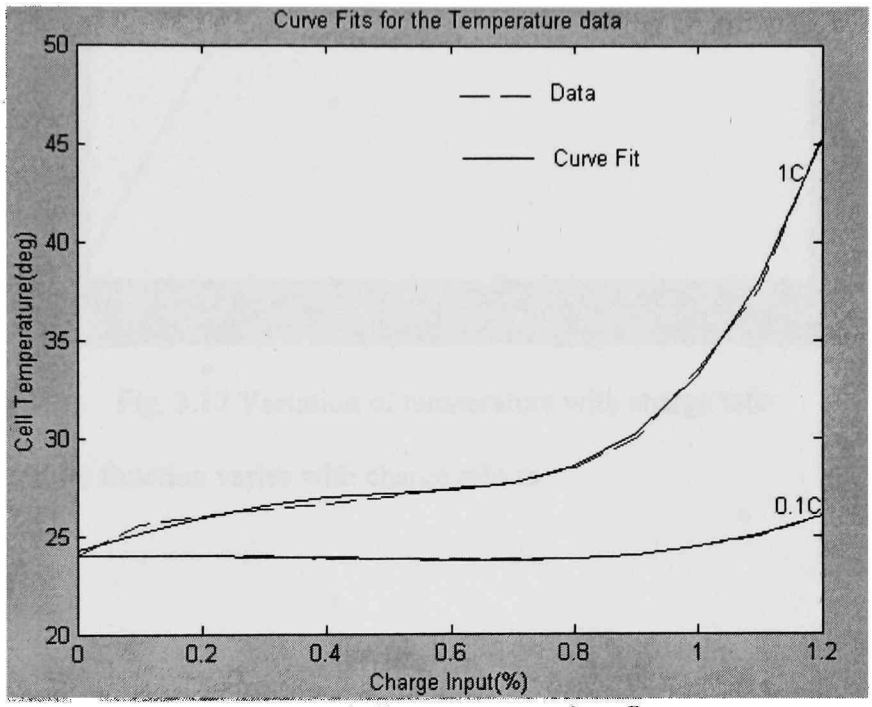

Fig. 3.16 Cell temperature data fits

be calculated. The type of interpolation used depends on the variation of temperature with the charge rate. Data points are chosen at 100% charge input for the temperature variation with charge rates at C/10, C/3 and C rates. Curve fitting of built-in non-linear models in Datafit at these three data points produced a best fit shown in Fig. 3.17 with a minimum error of -0.003484 and maximum residual error of 0.0021537 given as

$$T = 54.4929 - \frac{9.0144}{\sqrt{C_R}} . \qquad \text{----------3.14}$$

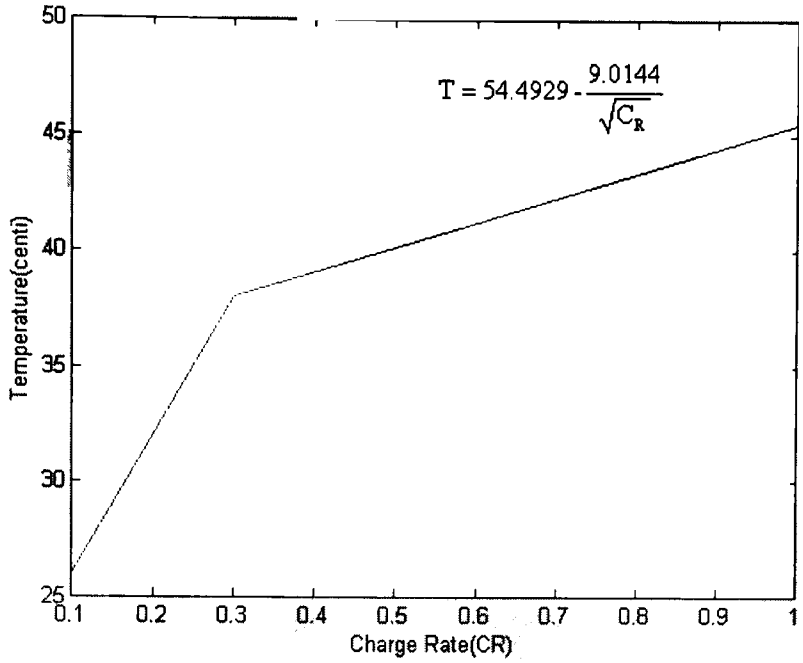

Fig. 3.17 Variation of temperature with charge rate

This temperature function varies with charge rate as

$$T = a + \frac{b}{\sqrt{C_R}}, \qquad \text{----------3.15}$$

where

T – is the temperature

C_R – is the charge rate.

Using equation 3.15 as interpolating function for C_R = C/10 and 1C charge rates gives

$$T_{0.1} = a + 3.16b \qquad \text{----------3.15a}$$

$$T_{10} = a + b. \qquad \text{----------3.15b}$$

Solving Eqs. 3.15a and 3.15b for 'a' and 'b' gives

$$a = T_1 + \frac{(T_1 - T_{0.1})}{2.16} \qquad \text{----------3.16a}$$

$$b = \frac{T_{0.1} - T_1}{2.16}. \qquad \text{----------3.16b}$$

Eq. 3.16 a and b are coefficients calculated, and substituting them into Eq. 3.15 gives the battery temperature rise in NiMH batteries as

$$T = T_1 - \left[\frac{(T_1 - T_{0.1})}{2.16}\left(\frac{1}{\sqrt{C_R}} - 1\right)\right], \qquad \text{----------3.17}$$

where

$T_{0.1}$ and T_1 – are temperature data fits as a function of charge input at 0.1C and 1C charge rates given as

$$T_1 = 270.86e^{C_1} - 246.617 - 263.4312C_1 - 95.6574C_1^2 - 97.327C_1^{2.5} \qquad \text{----------3.18a}$$

$$T_{0.1} = 42.9212e^{C_1} - 18.92136 - 41.17257C_1 - 9.8786C_1^{1.5} - 22.313C_1^{2.5}. \qquad \text{----------3.18b}$$

T_1 and $T_{0.1}$ are the curve fits for the temperature data shown in Fig. 3.16. These curves look exponential, but an exponential form doesn't fit the data properly. An exponential model of the form $e^{(a+bx)}$ which was tried to fit the data resulted in minimum and maximum residuals of -3.607 and 6.8, as can be seen in Fig. 3.18, which is not acceptable. The best-chosen curve fit is a combination of exponential and polynomial fits given by Eq. 3.18a and 3.18b. This model was chosen from TableCurve 2D which gave the least error for both charge rates. The minimum and maximum residuals for T_1 are -0.007522 and 0.032 and -0.0011765 and 0.05876 for $T_{0.1}$. Substituting Eq. 3.18a and

3.18b in Eq. 3.17 gives the relation for cell temperature rise in the NiMH battery during charging as

$$T = 70.86e^{C_1} - 246.617 - 263.4312C_1 - 95.6574C_1^2 - 97.327C_1^{2.5} - \left[\frac{\left(227.93\, e^{C_1} - 227.7 - 222.25C_1 + 9.878C_1^{1.5} - 95.6575C_1^2 - 75.014C_1^{2.5}\right)}{2.16}\left(\frac{1}{\sqrt{C_R}} - 1\right)\right]^{\cdot} \quad \text{----------3.19}$$

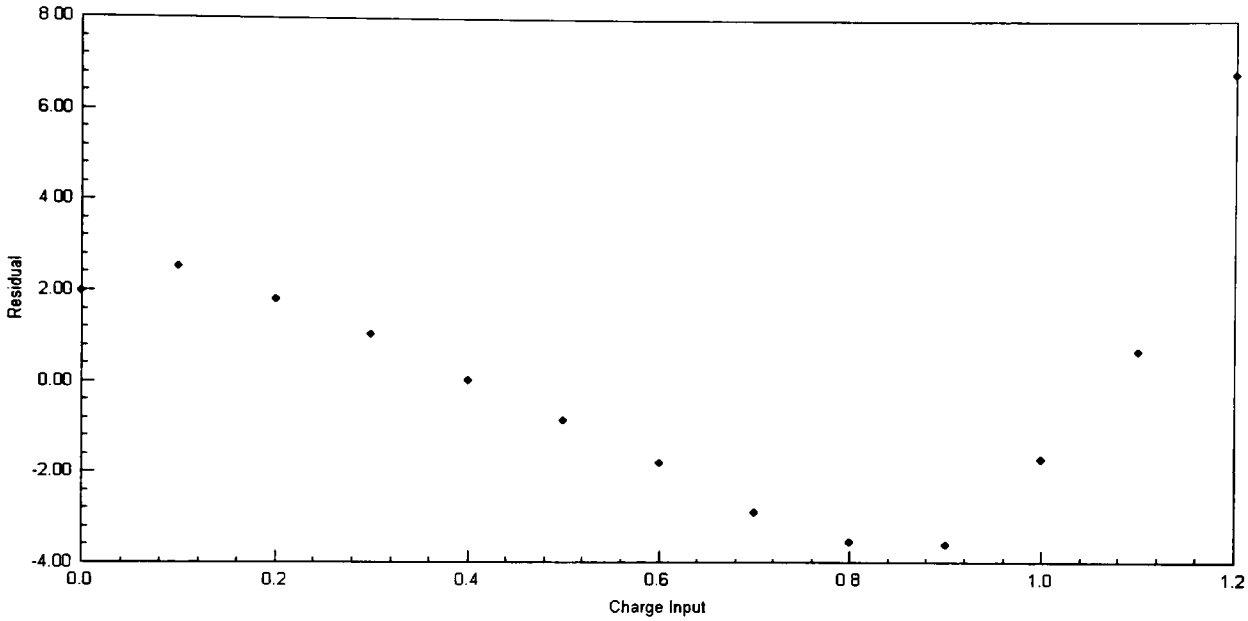

Fig. 3.18 Residuals of an exponential model.

Eq. 3.19 is modeled in simulink with charge input and charge rate as inputs to the block and cell temperature as the output. The various math functions and constant blocks in the simulink model are used as a part of Eq. 3.19. The two functional blocks contain the expressions given in Eq. 3.18a and Eq. 3.18b. They are written in the simulink model to indicate the individual functions. The following block incorporates the functional values of temperature rise for in-between charge rate intervals. Dumping more amp-hrs into the model creates a thermal runaway condition.

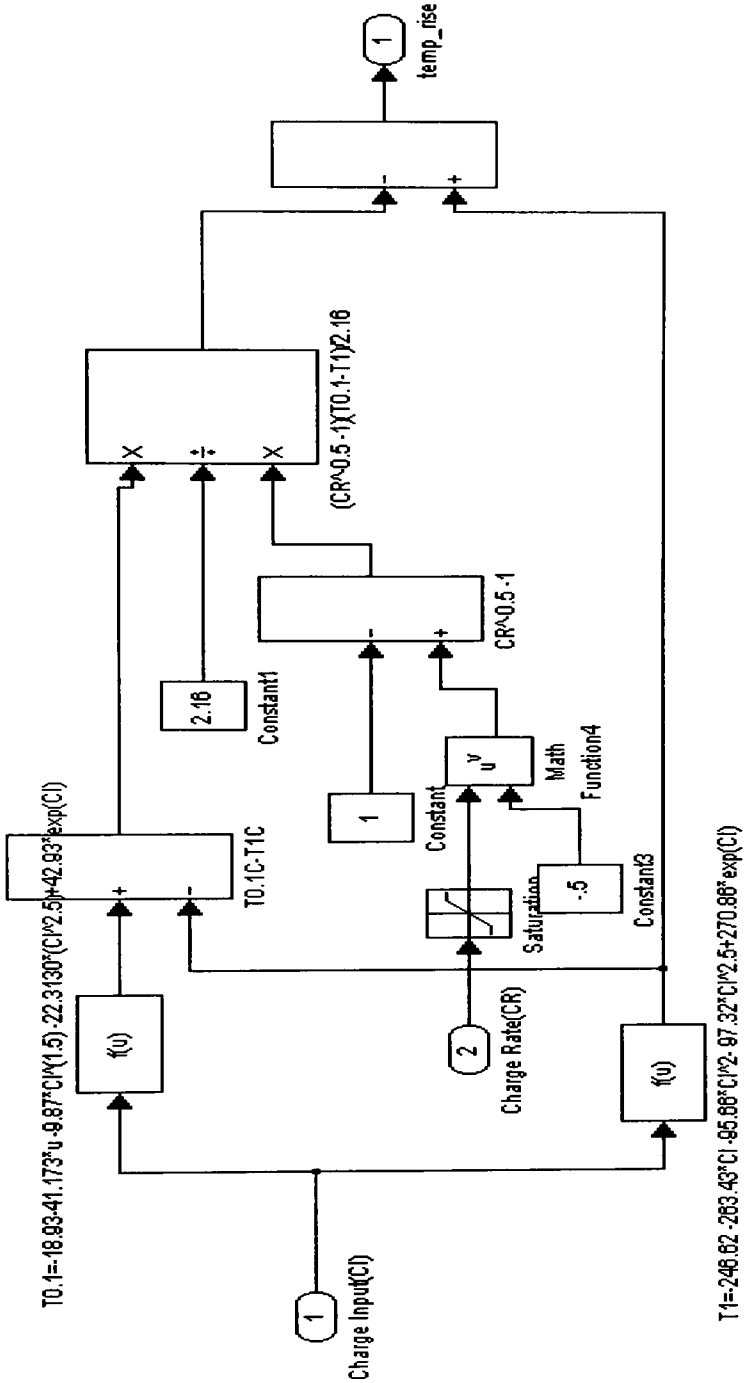

Fig. 3.19 Battery temperature block

3.2.3 Modeling the Pressure Block

The pressure block is modeled by an empirical equation from data

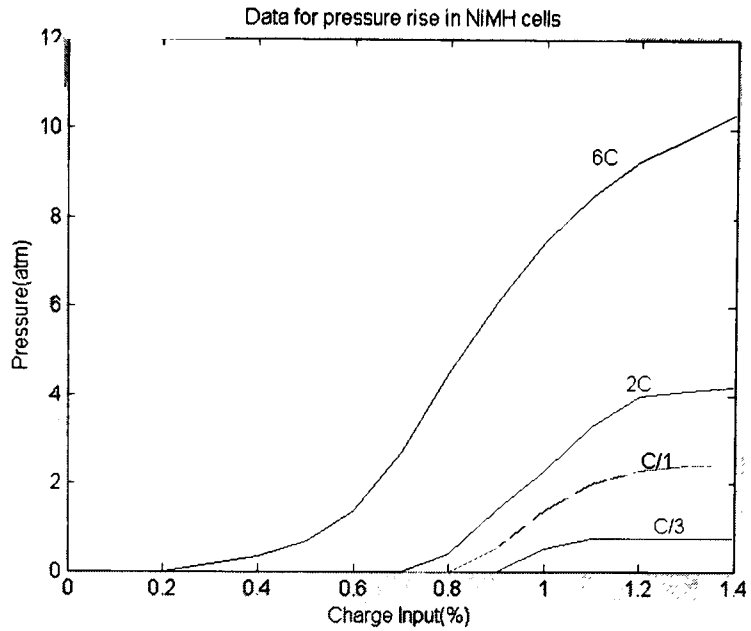

Fig. 3.20 Data used to model the pressure rise

as shown in Fig. 3.20[11]. Interpolation is used to find the functional values of pressure for in-between charge rate intervals. The interpolation method varies with the variation in pressure and charge rate considering the data points at a specified charge input. At 100% of charge input, this variation of cell pressure with charge rate is observed at C/3, C/1,2C and 6C charge rates. This data is run on Datafit to solve for non-linear models. This non-linear regression produced a minimum and maximum residual error of -0.001959 and 0.00350946 for Eq. 3.20.

$$P = -0.91882 + 0.035311C_R^2 \log(C_R) + 2.9153\sqrt{C_R} \qquad \text{----------3.20}$$

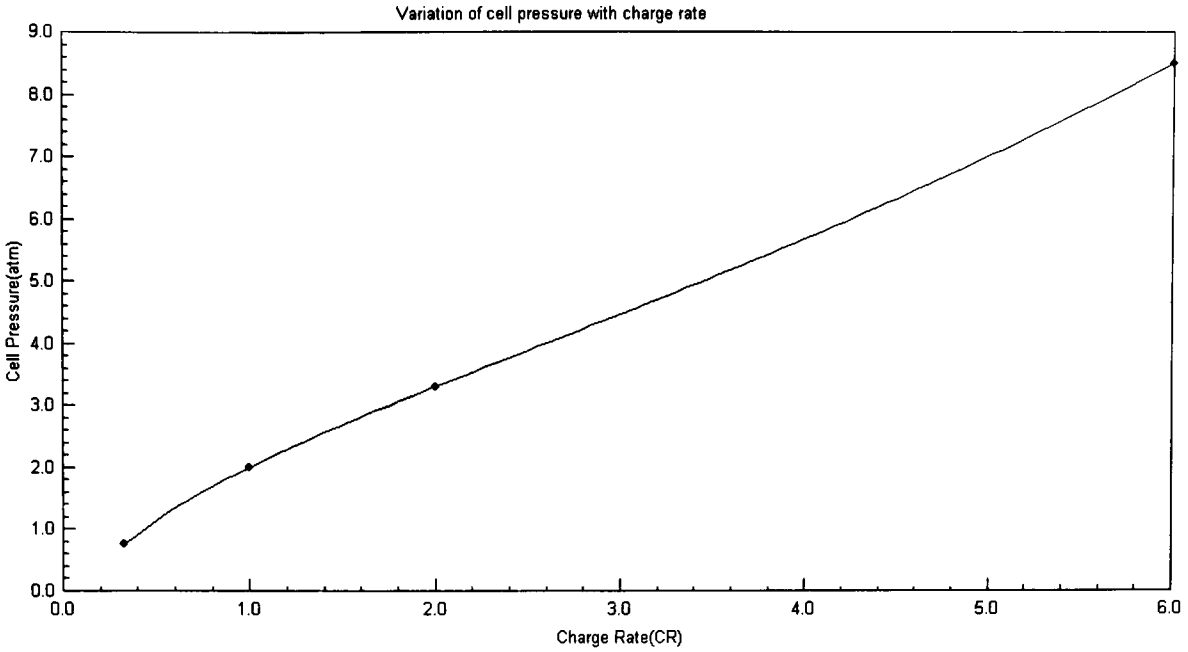

Fig. 3.21 Cell pressure variation with charge rate (C_R)

With this variation of pressure with charge rate, a general form of the equation is used as a method of interpolation to model the pressure block. The general form of this equation is

$$P = a + bC_R^2 \log(C_R) + c\sqrt{C_R} \qquad \text{----------3.21}$$

a, b and c are the fit coefficients.

Using C_R=0.33,2 and 6 in Eq. 3.21 yields a system of three equations as,

$$P_{0.33} = a - 0.052b + 0.574c \qquad \text{----------3.21a}$$

$$P_2 = a + 1.2b + 1.414c \qquad \text{----------3.21b}$$

$$P_6 = a + 28.01b + 2.45c\,. \qquad \text{----------3.21c}$$

Solving Eq. 3.21 (a-c) for the three coefficients 'a', 'b' and 'c' gives

$$a = 0.037P_6 - 0.829P_2 + 1.78P_{0.33}$$ ----------3.22a

$$b = 0.0395P_6 - 0.0884P_2 + 0.0489P_{0.33}$$ ----------3.22b

$$c = -0.058P_6 + 1.313P_2 - 1.264P_{0.33}.$$ ----------3.22c

Eq. 3.22(a-c) are fit coefficients 'a', 'b' and 'c' for the empirical equation of pressure. Substituting these coefficients into $P = a + bC_R^2 \log(C_R) + c\sqrt{C_R}$ (Eq. 3.21) gives the battery pressure rise in NiMH cells as

$$P = (0.03722P_6 - 0.8285P_2 + 1.7933P_{0.33}) + (0.0395P_6 - 0.0884P_2 + 0.0489P_{0.33})C_R^2 \log(C_R) + (-0.0579P_6 + 1.3127P_2 - 1.264P_{0.33})\sqrt{C_R},$$

----------3.23

where

$P_{0.33}$, P_2 & P_6 - are the fit equations for the pressure at various charge rates, which are functions of charge input given as

$$P_{0.33} = -4.95C_I^5 + 13.38C_I^4 - 10.67C_I^3 + 2.74C_I^2 - 0.11C_I - 0.006$$

----------3.24a

$$P_2 = -126.38C_I^9 + 769.65C_I^8 - 1860.9C_I^7 + 2262.9C_I^6 - 1447.6C_I^5 + 464.19C_I^4 - 59.567C_I^3 - 0.43183C_I^2 + 0.38967C_I - 0.001318$$

----------3.24b

$$P_6 = -66.803\,C_I^7 + 369.92C_I^6 - 784.23C_I^5 + 785.16C_I^4 - 371.74C_I^3 + 81.292C_I^2 - 6.1135C_I^2 + 0.018277\ .$$

----------3.24c

Eq. 3.24 a, b and c are polyfits generated in Matlab (Fig. 3.22). The norm of residuals for the three charge rates is 0.09786, 0.0176, and 0.0988. Substituting these fit equations in Eq 3.23 gives the battery pressure. The simulink model is shown in Fig. 3.23. The inputs are the charge rate C_R and charge input C_I and output is pressure. The

math functions and constants shown in the model are a part of Eq. 3.23. The functional blocks 'a', 'b' and 'c' are used for the expressions shown in Eq. 3.22 a, b and c. All the equations developed are referenced in the simulink model.

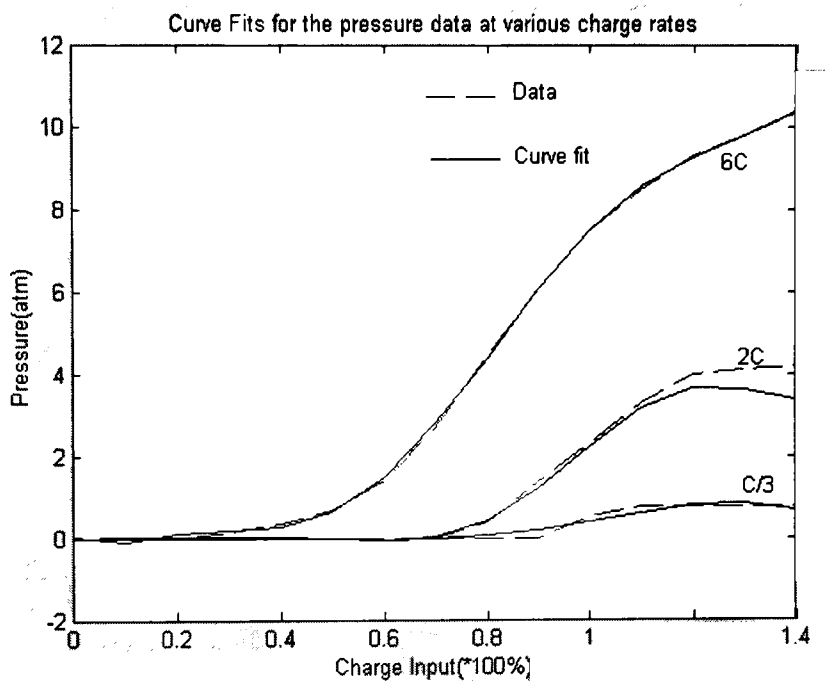

Fig. 3.22 Polynomial data fits for the cell pressure at various charge rates.

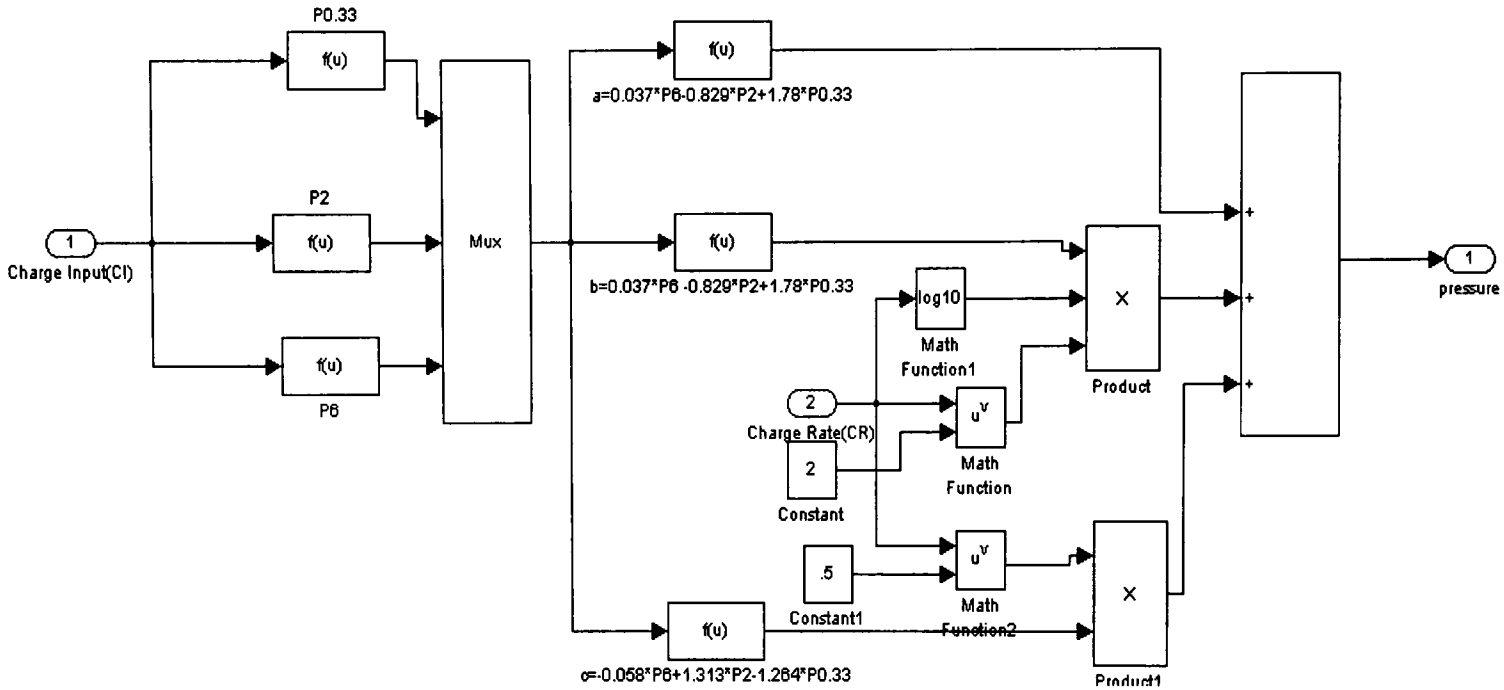

P0.33=-4.95*CI^5 + 13.38*CI^4 -10.68*CI^3 + 2.74*CI^2 -0.11*CI^1 -0.0065

P2=-126.38*CI^9 +769.65*CI^8 -1860.9*CI^7 + 2262.9*CI^6 -1447.6*CI^5 + 464.19*CI^4 -59.567*CI^3 -0.43*CI^2 +0.39*CI^1 -0.0013

P6=-66.803*CI^7 + 369.92*CI^6-784.23*CI^5 + 785.16*CI^4-371.74*CI^3 + 81.292*CI^2 -6.1135*CI^1 + 0.018277

Pressure=a+(b(CR^2)*(log(CR)))+c*(CR^0.5)

Fig. 3.23 Pressure block

3.3 Discharge Model of NiMH Battery

The model estimates voltage during discharge at various discharge rates. Manufacturers' measured data was used to derive the relations for capacity discharged and discharge voltage at 20^0C. In Fig. 3.24, the battery model is described as having the battery discharge current and nominal amp hr capacity as inputs, and the battery voltage as the output. The discharge curves are modeled using an empirical equation for discharge voltage for various intervals of discharge rates from data shown in Fig. 3.25.

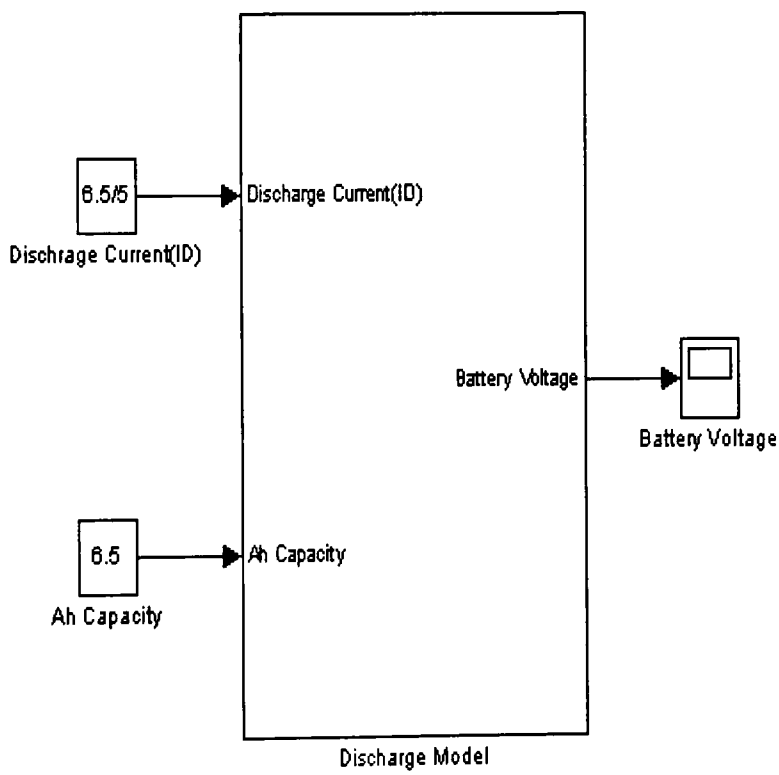

Fig. 3.24 Top-level discharge model

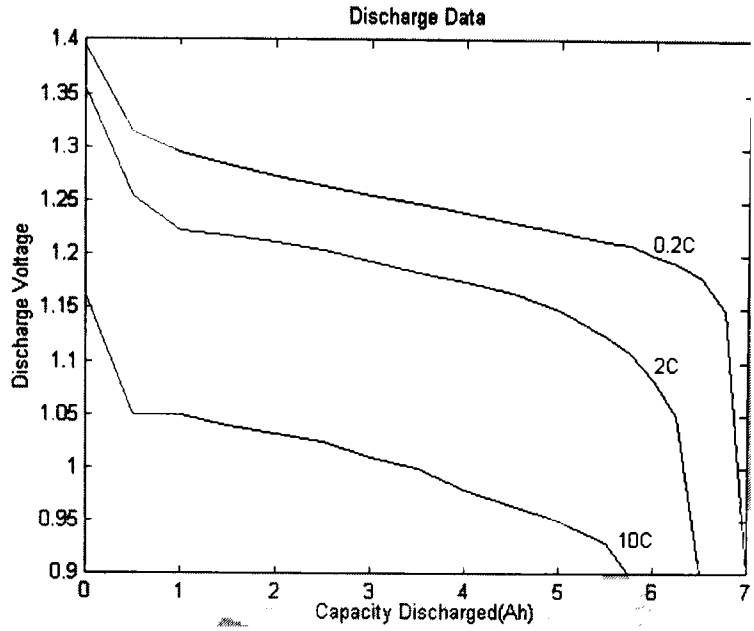

Fig. 3.25 Discharge data

3.3.1 Capacity Block

The principal environmental influence on the shape of the voltage profile is the discharge rate. As with the voltage profile, the capacity available (CA) during a discharge is dramatically affected by rate of discharge. Fig. 3.26 shows how discharge rate influences these two factors. The available capacity varies with the discharge rate as shown in Table 3.1 [13].

Table 3.1 Capacities available at various discharge rates [13]

Discharge Rate(C)	0.2	1	2	5	10
Available Capacity(Ah)	7	6.76	6.5	6.25	5.75

The rated capacity of this battery is 6.5Ah. Using Table 3.1, an empirical equation of available capacity is found using Datafit. A simple non-linear model (built-in model in Datafit) is chosen which nearly fits the data. The minimum and maximum residual errors are -0.00913 and 0.007966 justifying the use of this model as

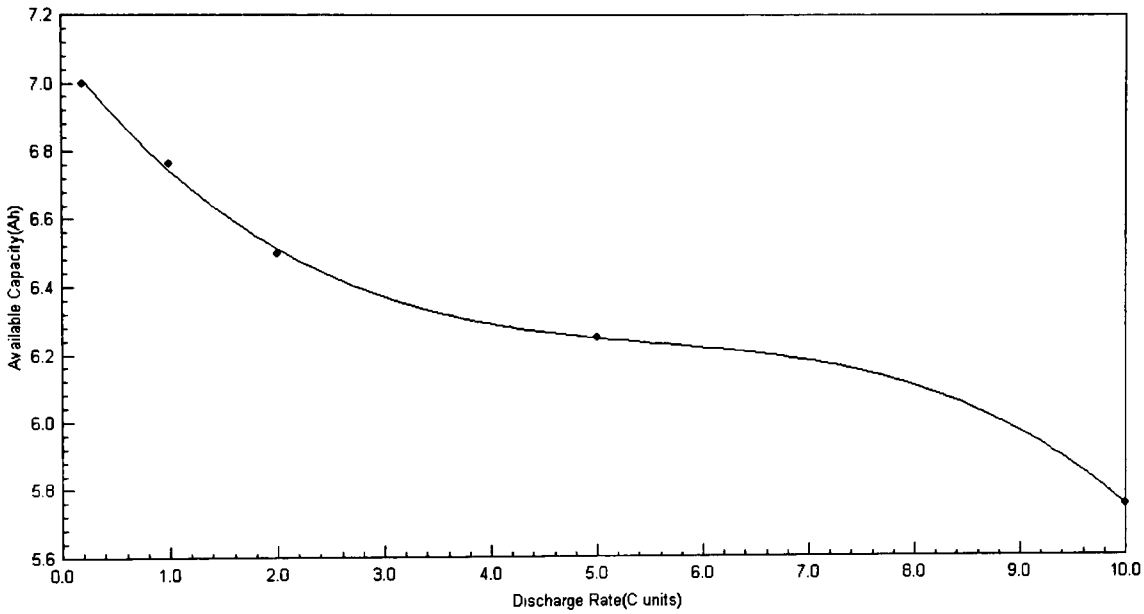

Fig. 3.26 Variation of available capacity (CA) with discharge rate (D_R)

$$CA = -0.00410376\,D_R^3 + 0.06839D_R^2 - 0.407266\,D_R + 7.08747, \qquad \text{----------3.25}$$

where

CA - is the capacity available (Ah)

D_R is the discharge rate (C units).

If 'CA' indicates the available capacity at a given discharge rate, the depth of discharge (D) is given by [14],

$$D = \frac{CA}{6.5}\int \frac{I_D}{(3600 \times 6.5)} dt . \qquad \text{----------3.26}$$

For example, if the battery is discharged at a rate C/5 rate, the available capacity is 7Ah, which means the depth of discharge can go to 108% before the end point of 0.9V is reached. The empirical equations for voltage profiles in the following sections are modeled as a function of depth of discharge, 'D'. Eq. 3.26 is shown in simulink in Fig. 3.27.The saturation block is used since the data is restricted between 0.2C and 10C discharge rates. The capacity available equation is shown with the variable name 'CA' in the model.

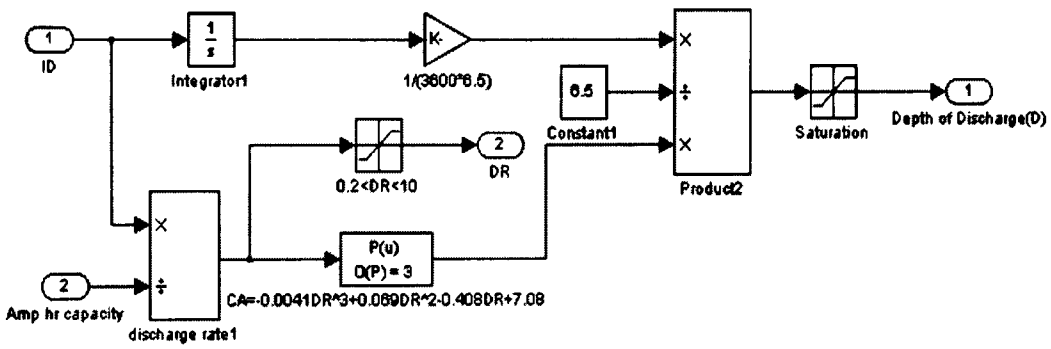

Fig. 3.27 Depth of discharge block

3.3.2 Voltage Block

The voltage block models the empirical equation for voltage using the data shown in Fig. 3.25 for various discharge intervals through interpolation techniques. The inputs to the model are the depth of discharge (D) and discharge current (I_D) shown in Fig. 3.24. The interpolation method is chosen depending on the variation of voltage with discharge rate. Sample voltage points are chosen at 89% depth of discharge for five discharge

intervals at C/5, C/1,2C, 5C and 10C and a model equation is chosen to fit the data (Fig. 3.28) using Datafit software. The data is plugged into Datafit software for a proper curve fit. The model is chosen by verifying the residual errors.

$$V = \frac{1}{\left(0.8 - 0.02467D_R - 0.000285D_R^2\right)} \qquad \text{----------3.27}$$

Eq. 3.27 has minimum and maximum residual errors of -0.0001858 and 0.0002787 and was considered the best fit. The general form of Eq. 3.27 considered is

$$V = \frac{1}{\left(a + bD_R + cD_R^2\right)}. \qquad \text{----------3.28}$$

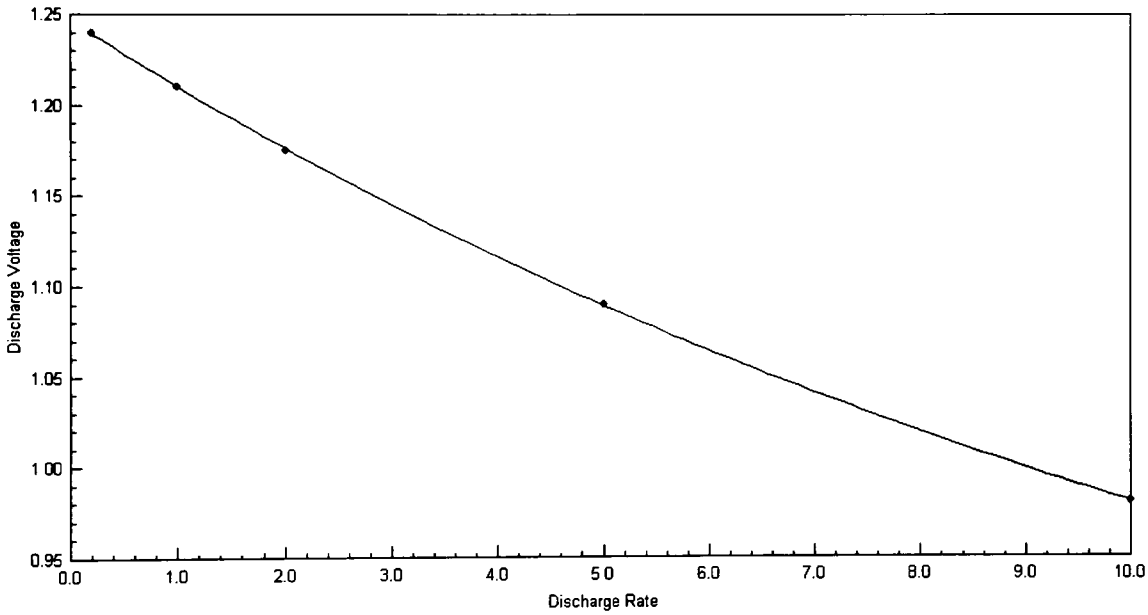

Fig. 3.28 Variation of voltage with discharge rate

This gives the voltage characteristic with discharge rate which is used to interpolate for various discharge intervals. For accuracy of interpolation, Eq. 3.28 is used with three

discharge rates at C/5,2C and 10C. Substituting into Eq. 3.28 and solving for 'a', 'b' and 'c' gives

$$a = \frac{1.13}{V_{0.2}} - \frac{0.14}{V_{.2}} \qquad \text{----------3.28a}$$

$$b = \frac{-0.68}{V_{0.2}} + \frac{0.7083}{V_2} - \frac{0.028}{V_{10}} \qquad \text{----------3.28b}$$

$$c = \frac{0.0567}{V_{0.2}} - \frac{0.06945}{V_2} + \frac{0.012755}{V_{10}} \qquad \text{----------3.28c}$$

where

$V_{0.2}$, V_2 and V_{10} – are the data fits for voltage at C/5,2C and 10C discharge rates given as

$$V_{0.2} = -2488.6D^{10} + 12778D^9 - 27905D^8 + 33762D^7 - 24690D^6 + 11156D^5 - 3042.9D^4 + 460.52D^3 - 29.815D^2 - 0.41404D^1 + 1.395 \qquad \text{----------3.29a}$$

$$V_2 = -13.52D^5 + 32.71D^4 - 29.11D^3 + 11.571D^2 - 2.1D + 1.357 \qquad \text{----------3.29b}$$

$$V_{10} = 15.3D^8 - 102D^7 + 263.06D^6 - 347.5D^5 + 257.11D^4 - 108.12D^3 + 24.63D^2 - 2.77D + 1.162. \qquad \text{----------3.29c}$$

These empirical equations are polynomial fits generated in Matlab. Various degrees of polyfits were tried and the one with minimum error was chosen. Eq. 3.29(a-c) came with minimum and maximum residuals of-0.007925 and 0.006396, -0.0018 and 0.00218, -0.00673 and 0.00982 justifying the best fit for the data. Substituting 'a', 'b' and 'c' into Eq. 3.28 gives the expression for voltage as

$$V = \frac{1}{\left(\left(\frac{1.13}{V_{0.2}} - \frac{0.14}{V_{.2}}\right) + \left(\frac{-0.68}{V_{0.2}} + \frac{0.7083}{V_2} - \frac{0.028}{V_{10}}\right) D_R + \left(\left(\frac{0.0567}{V_{0.2}} - \frac{0.06945}{V_2} + \frac{0.012755}{V_{10}}\right) D_R^2\right)\right)}$$

----------3.30

Fig. 3.29 models Eq. 3.30 in simulink. The functional blocks a, b, c in the model include the parameters 'a', 'b' and 'c' referenced at the bottom of the model (Eq. 3.29(a-c)) and other math functions to model the relevant relations. The input 'D' is the depth of discharge from the capacity block (Eq. 3.26). For various discharge intervals the block incorporates the voltage profiles. The other input shown is the discharge rate, D_R. However, this relation is restricted for $0.2C \leq D_R \leq 10C$. The following chapters deal with the simulation results and validation.

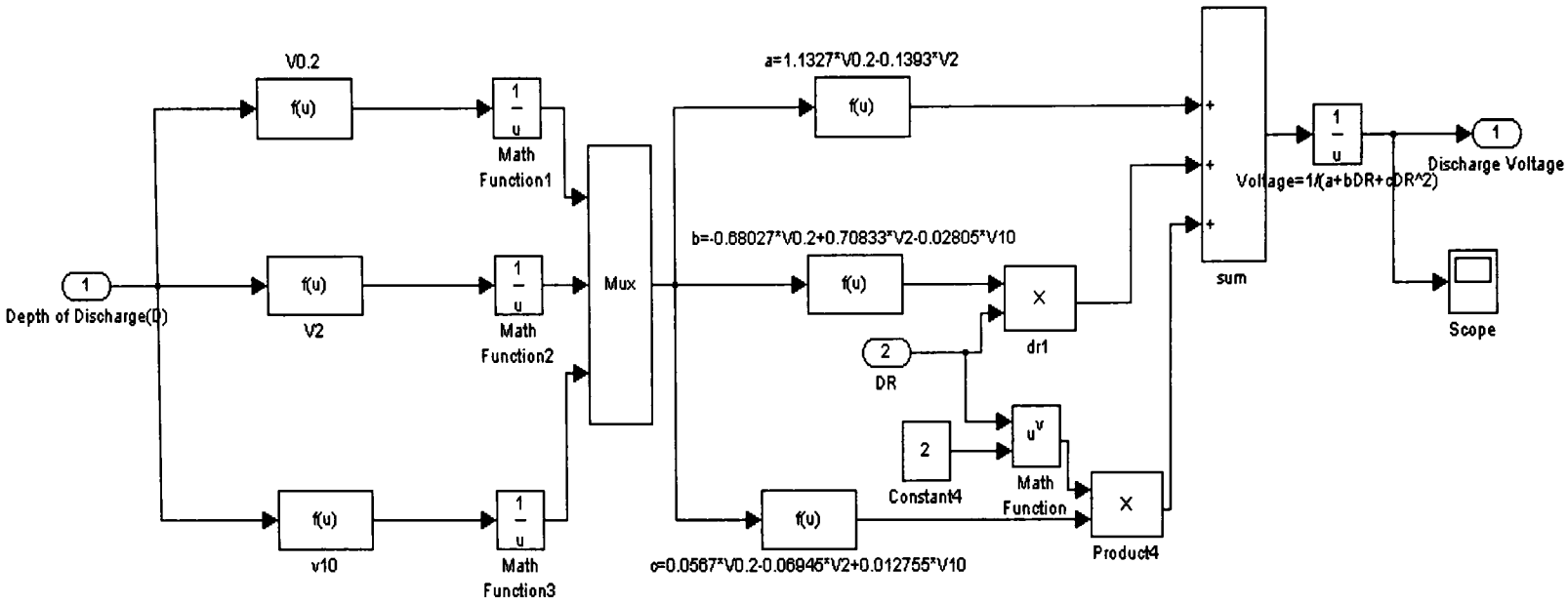

V0.2=-2488.6*D^10 + 12778*D^9 -27905*D^8 + 33762*D^7 -24690*D^6 + 11156*D^5-3042.9*D^4 +460.52*D^3 -29.815*D^2 -0.414040*D^1 +1.3949

V2=-13.522*D^5 +32.709*D^4 -29.102*D^3 + 11.571*D^2 -2.0923*D^1 + 1.3569

V10=15.301*D^8 -101.98*D^7 +263.06*D^6 -347.5*D^5 +257.11*D^4 -108.12*D^3 +24.63*D^2 -2.7707*D^1 +1.1623

Fig. 3.29 Simulink model of discharge voltage

CHAPTER IV

SIMULATION RESULTS

The charging and discharging models developed in the previous chapter are combined together to get a battery pack model which was tested for several charge and discharge cycles. Both the charge and discharge models are developed based on their specifications and data. For verification, a battery pack consisting of 40 series battery modules was used, since this represents the size pack used in an HEV. Each battery module is 7.2 volts, or 6 series cells, and has a capacity of 19.5 Ah. Since the data for the models developed were for a single cell, they were scaled to fit the battery pack.

4.1 Simulation of the Battery Model

The overall battery model is shown in Fig. 4.1. The input references are three cycles of discharge and charge currents. Using these inputs, state of charge, battery voltage, charge efficiency, pressure and temperature are observed to see how the individual models function. The input amp-hr capacity is 19.5Ah and the initial state of charge is assumed to be 70%. Fig. 4.2 shows the inside of the top-level model with individual subsystems.

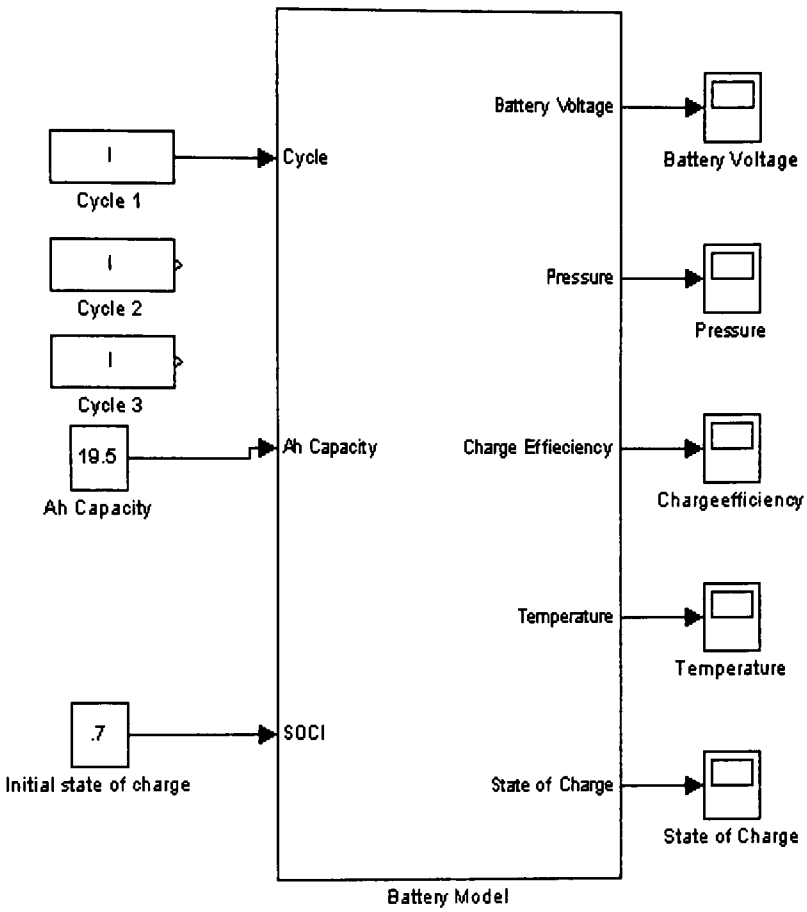

Fig. 4.1 Battery simulink model

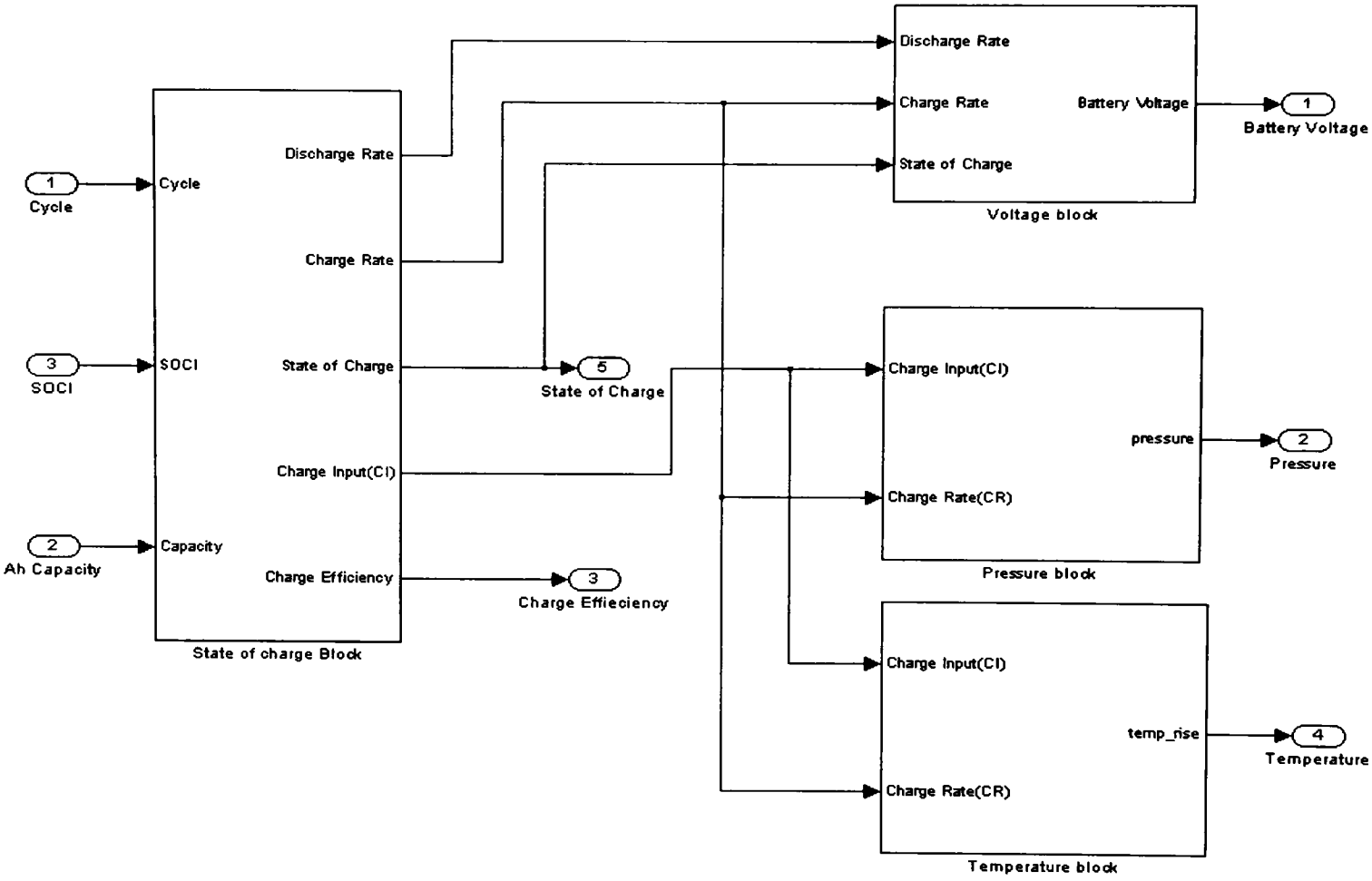

Fig. 4.2 Sub system model of battery

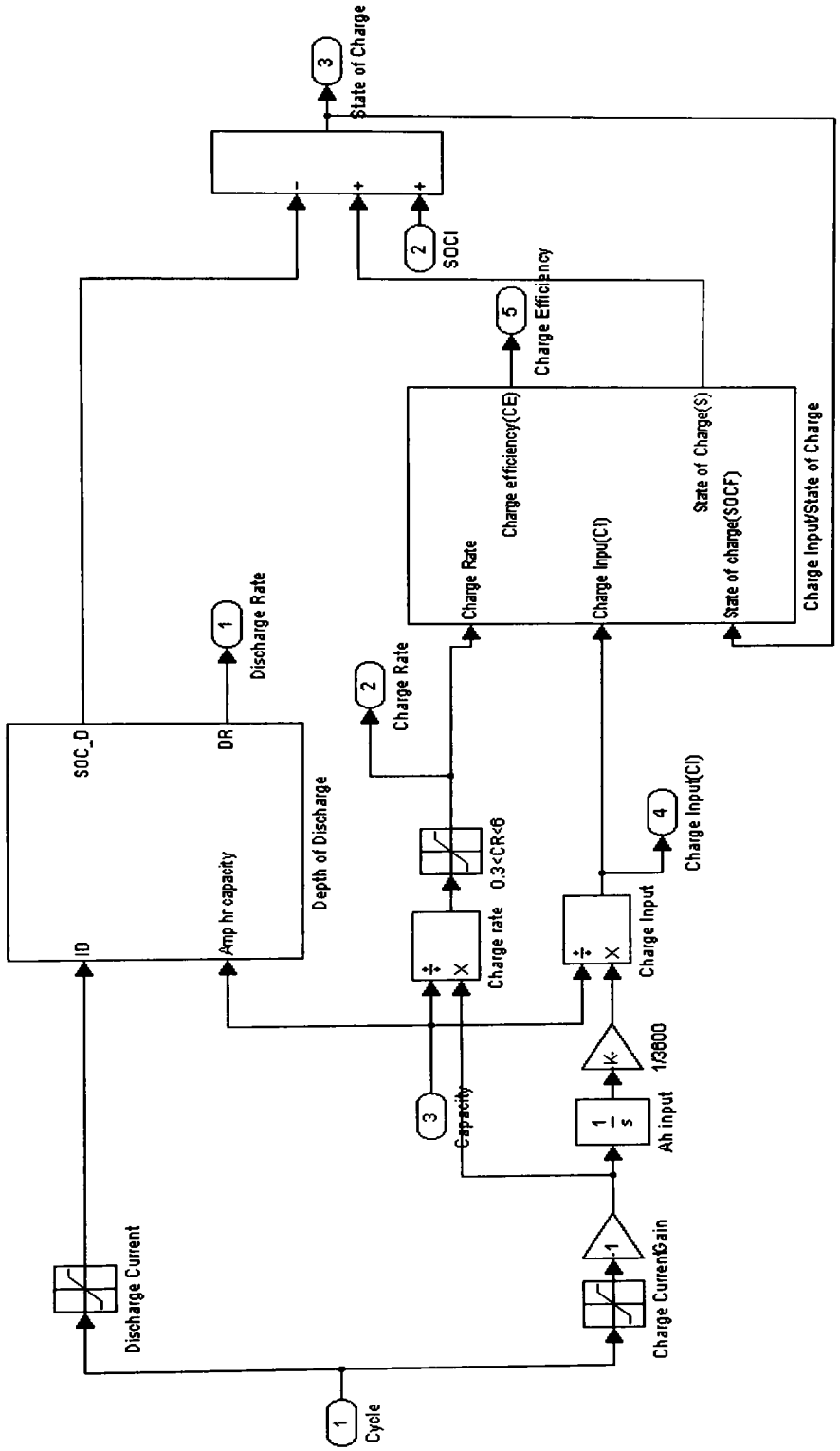

Fig. 4.3 State of charge during charge and discharge

Fig. 4.3 shows the state of charge block in the battery model. (The two sub systems shown in Fig. 4.3 are explained and shown in Chapter III) Following are the list of equations governing the state of charge of Fig. 4.3.

$$SOC_F = SOC_I - SOC_D - SOC_C \quad \text{---------- 4.1}$$

SOC_F - is the final state of charge

SOC_I - is the initial state of charge

SOC_D - is the decrement in percentage of charge during discharge period (DOD)

SOC_C - is the increment in percentage of charge during charge period

$$SOC_D = \frac{CA}{6.5}\int \frac{I_D}{(3600 \times 6.5)} dt \quad \text{---------- 4.2}$$

$$SOC_C = CE \times \frac{1}{C_P}\int \frac{I_C}{3600} dt \quad \text{---------- 4.3}$$

C_P - is the amp-hr capacity equal to 19.5Ah

I_C and I_D are charge and discharge currents.

The input to the model is a cycle of charge and discharge currents. A positive input of current is assumed when the battery is discharging and negative input of current when it is charging. The two saturation blocks in the model divide the input current into charge and discharge currents. The first saturation block accepts the positive current which is discharge current I_D, the second saturation block accepts negative current which is charge current, I_C. Based on the timing, the battery switches between charge and discharge cycles. Eq. 4.2, SOC_D gives the percentage of charge (0-100%) lost during

discharge and Eq. 4.3, SOC_C gives the percentage of charge added (0-100%) during the charging phase.

4.2 Simulation Results

4.2.1 State of Charge and Charge Efficiency

The reference input to the battery model for a typical charge and discharge cycle is shown in Fig. 4.4. State of charge of the battery pack is shown in Fig. 4.5. The initial

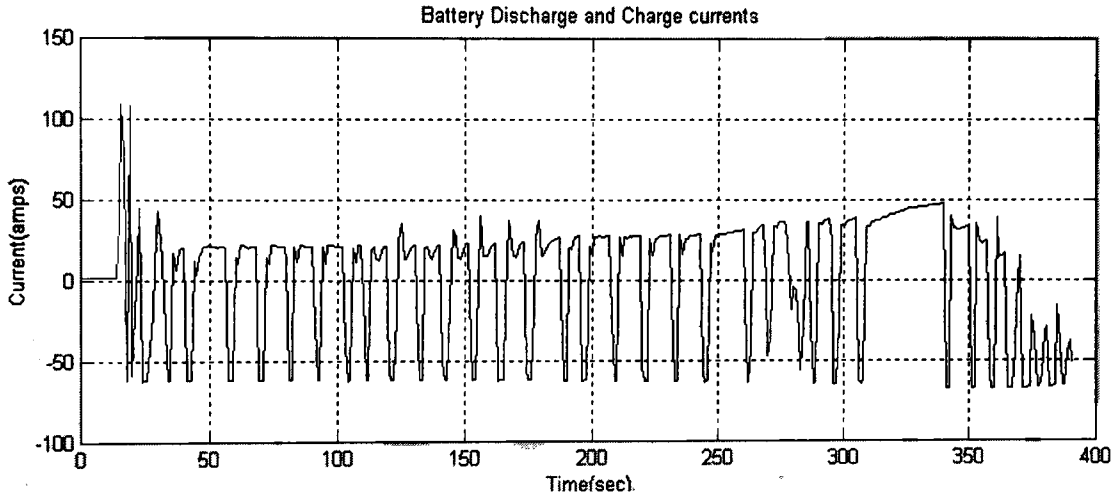

Fig. 4.4 Discharge and charge current cycle

state of charge is chosen as 70%. The state of charge responds to the sudden high discharge current after 15secs. During this period, as mentioned in Eq. 4.2 there is an amount of charge lost and the state of charge starts decreasing. Thereafter, when the discharge current goes to zero and battery is getting charged, the state of charge increases. However, this increase in state of charge is not linear with the increase in percentage amount of charge input. This is because the actual state of charge is not equal to charge input. For example, in Fig. 4.6 at t=18s the battery starts charging and reaches a

highest charge rate of 3.19C. At this point for state of charge equal to 70%, the charge efficiency drops to 90%, the simulation result is shown in Fig. 4.7. This happens frequently in the cycle because the charge rate keeps jumping between 0.1C to 3.19C.Due to the generation of oxygen, the charge acceptance efficiency decreases when it is

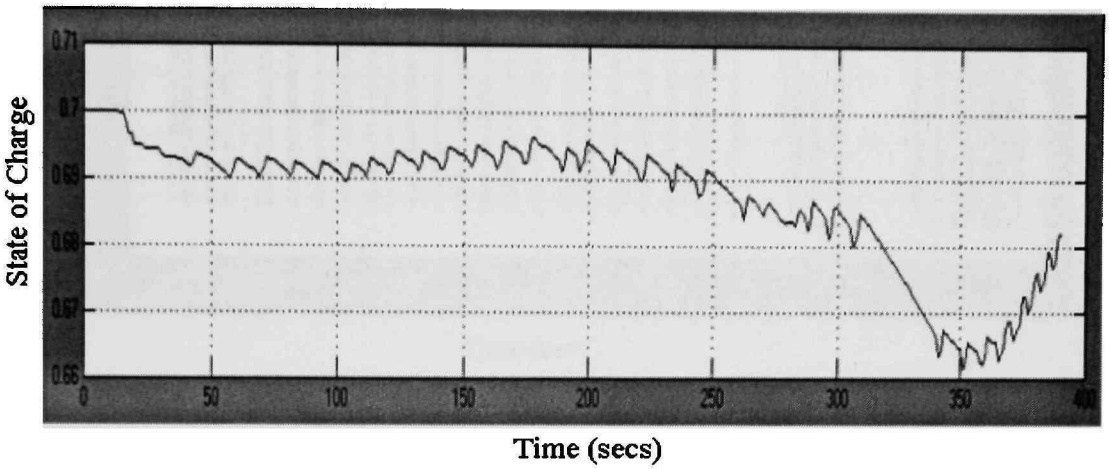

Fig. 4.5 State of charge variation during the cycle

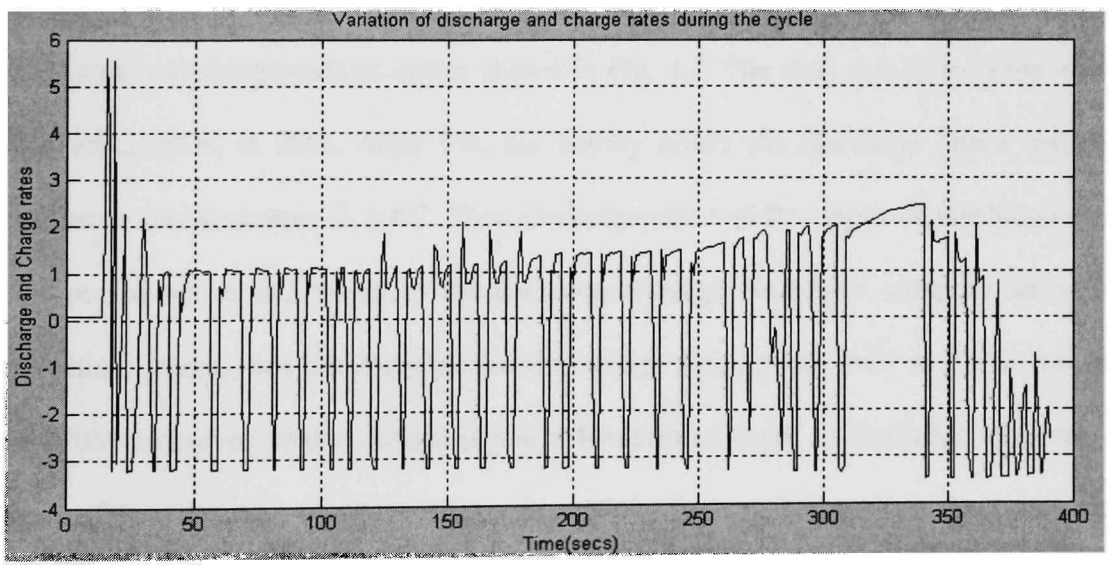

Fig. 4.6 Variation of discharge and charge rates during the cycle. (Positive values are the discharge rates and negative values are charge rates)

charging at 3.19C and effectively 100% charge is never achieved for 100% of the charge input when the charge rates are higher.

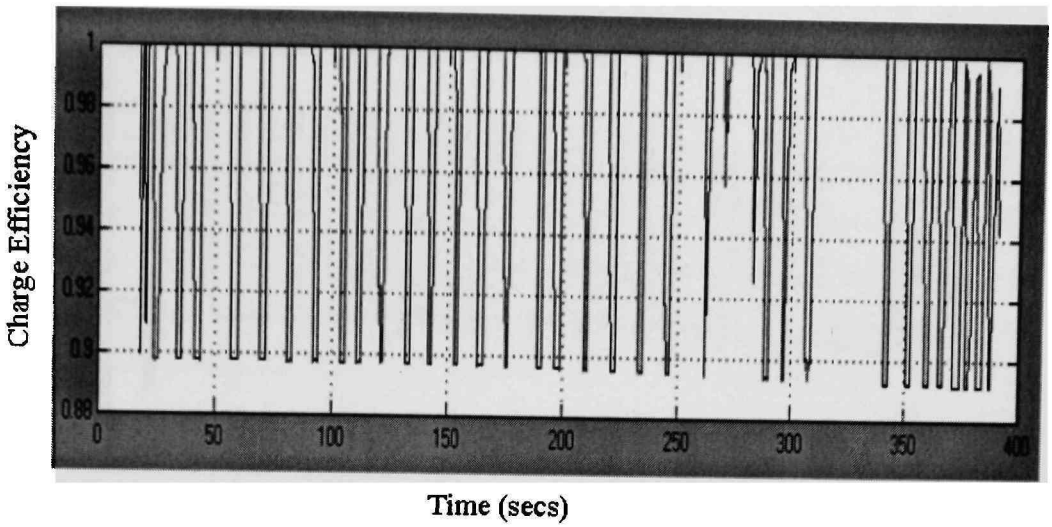

Fig. 4.7 Charge efficiency variation during charging periods

4.2.2 Battery Pack Voltage

Fig. 4.8 shows the simulated voltage profile of the NiMH battery pack during the discharge and charge current cycles shown in Fig. 4.4. The total simulation time is 391s. The initial SOC is 70%. After 15s, the battery enters the discharge phase, where its discharge rate increases to 5.6C. This discharge rate and the depth of discharge during this period act as the inputs to the discharge voltage block and compute the voltage transition. During this discharge period the voltage drops from 305V to the lowest point of 270V. However, if the voltage is just a function of depth of discharge, then the end point of this discharge would be higher than 270V. But since, it is a function of discharge rate and the battery is discharged at a higher rate, the voltage drops more quickly and the

end point reaches 270V. Later, the battery goes into the charging phase at a charge rate of 3.19C and reaches 380V during this peak power charge. The larger the charge rate is,

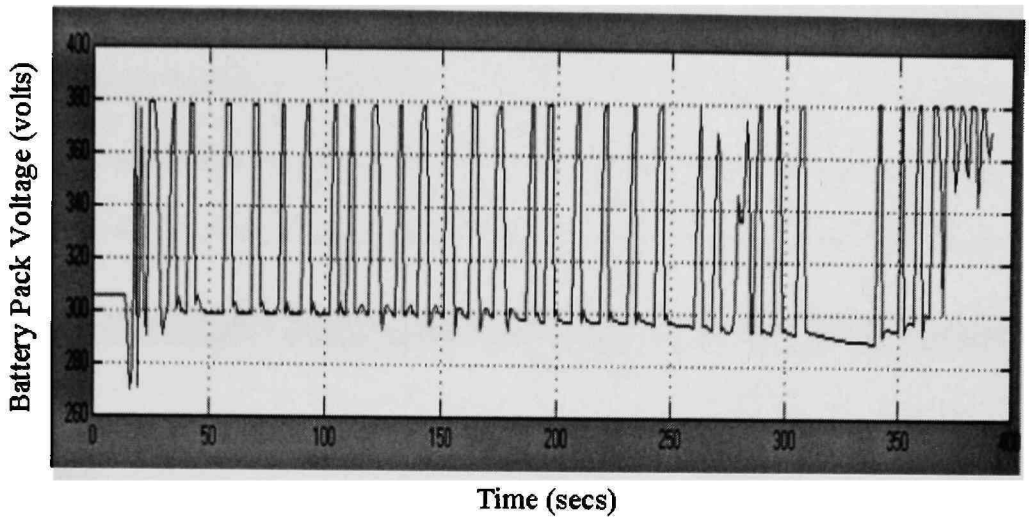

Fig. 4.8 Variation of battery voltage during discharge and charge cycles

the more quickly the voltage increases and the appearance of this peak voltage at each charge rate is different. This cycle continues with the battery charging and discharging at various rates.

4.2.3 Pressure Profiles

Fig. 4.9 is the simulation result of the battery pressure. It is assumed in this model that the oxygen gas is the only contributor to the battery pressure which occurs only during the charging and overcharging of the batteries. As considered earlier, the reference input to test the model consists of charge and discharge currents and hence, the pressure block responds only during the charging phase. The pressure block is modeled by an empirical equation which is a function of charge input and charge rate. However, the

magnitude of pressure rise is negligible in this case. If the battery would have been subjected to a constant charge, the battery pressure starts increasing. However, the cell pressure increases only after a certain point where the rate of oxygen generation at the nickel electrode begins to exceed the rate of oxygen recombination at the MH electrode [11]. This can be observed only after 100% of charge input when charged at low rates. However, in this case the charge input during the charging phase is just 10% of the rated

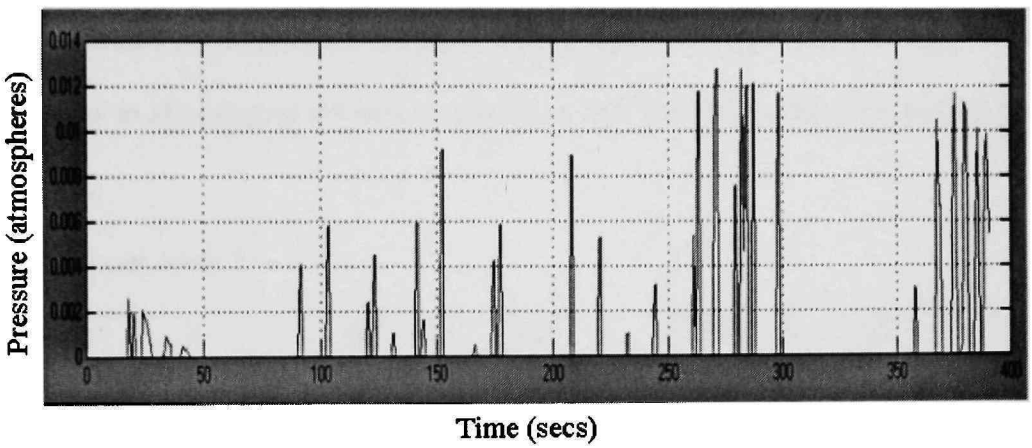

Fig. 4.9 Increase in battery pressure during charge

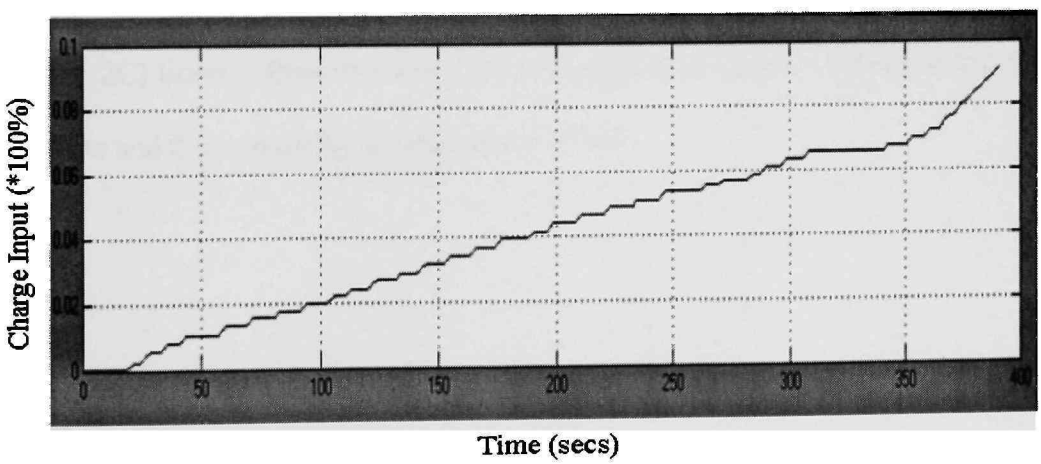

Fig. 4.10 Charge Input (percentage of rated capacity) for input cycle 1

capacity (Fig. 4.10) during the cycle of 391s and the charge rate is 3.19C, the cell pressure is negligibly small.

4.3 Simulation Results during Charge and Overcharge

The simulation results for battery pressure are discussed above for input cycle 1. However, since it's in discharging and charging phase, the effects of oxygen reactions of the NiMH battery are negligible .In order to better understand these issues, the simulation results are tested for another input cycle 2 which is just a charging cycle. Here the battery is subjected to charging at various charge rates and the results are analyzed for various parameters.

Table 4.1 Input cycle 2

Time(secs)	0	50	700	1100	1400	1700
Current(A)	0	0	40	100	117	95

As can be seen from Fig. 4.11 the battery starts charging with charge current increasing to 40A (2C) linearly from t= 50s to 700s.Thereafter the charge current increased to 117A (6C) rate and then gradually decreased at t=1700s.

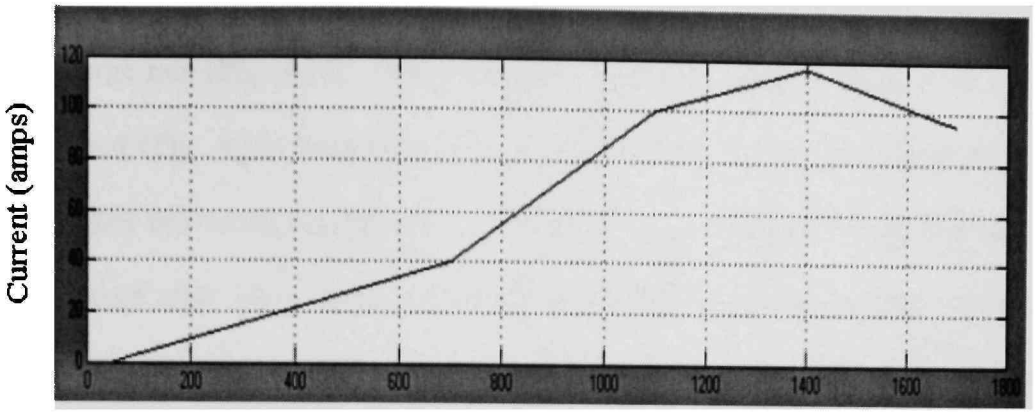

Fig 4.11 Current input cycle 2 (Battery subjected to overcharge)

The capacity of the cell is 19.5Ah.The battery is charged at higher rates ranging from 2C to 6C rate during this cycle and the battery is overcharge to 150% of its rated capacity as shown in Fig. 4.12.

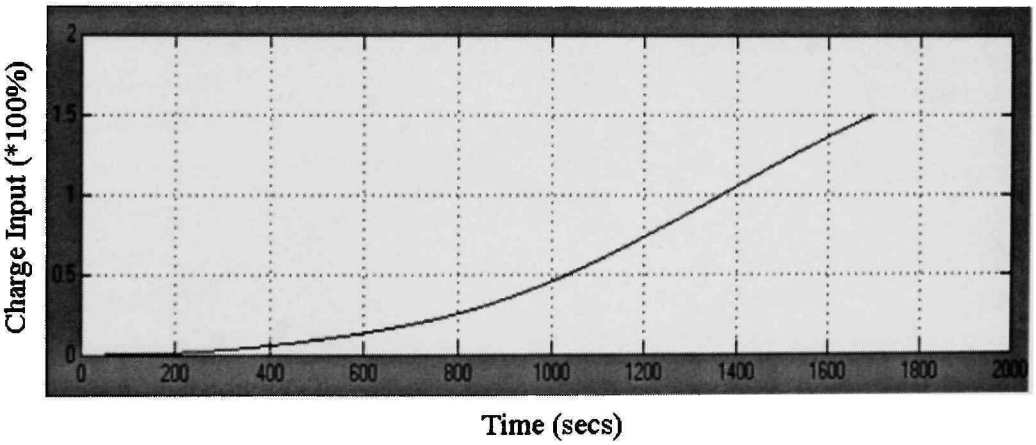

Fig 4.12 Charge input (0-150%) to the battery

The actual state of charge (Fig. 4.13) is not equal to the charge input due to oxygen generation in batteries. The battery state of charge decreases with oxygen generation rate because a smaller portion of current is actually used to charge the active materials [11].

This is clearly observed in this example. From t=700s to 1000s, the battery is charged at a higher charge rate (Fig. 4.11). At this time the gradual increase in the state of charge is now reduced (Fig. 4.13) because a part of input charge is now consumed to generate oxygen rather than charging the active materials, thus reducing the charge efficiency. In the later stage after 1400s when the charge rate is decreased the state of charge again increases. This implies that, at charge rates below 1C, the state of charge can approach 100% with 100% charge input while at higher rates the state of charge approaches 100% for 140% to 150 % of charge input. This implies that the cell usually has to be overcharged to an extent, which depends on the charge rate, to achieve full charge. The actual state of charge, however, did not always reach 100% as the charge acceptance efficiency decreases from 100%-0 %(Fig. 4.14).

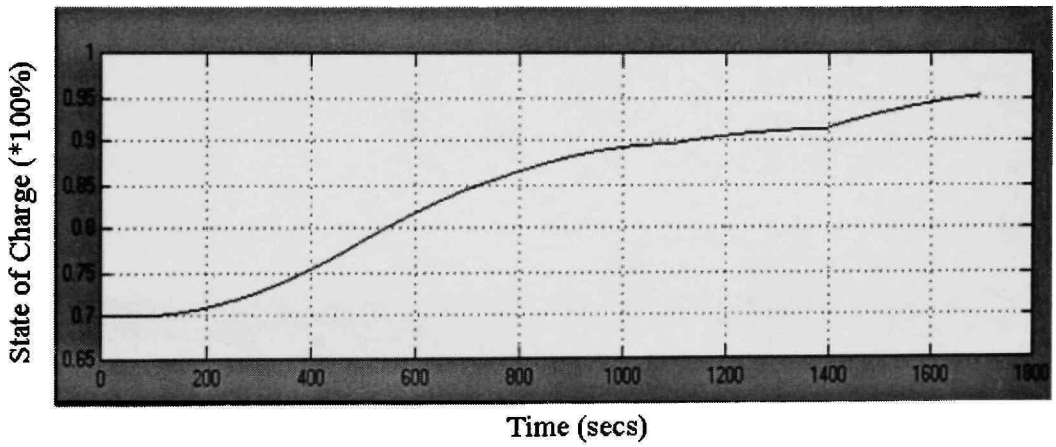

Fig 4.13 Increase in the state of charge during the charge cycle

It is obvious that the charge acceptance is strongly dependent on the state of charge. When the state of charge exceeds 80%, oxygen starts evolving significantly at charge rates as low as C/3 and even before at higher rates [11]. This can be observed

from Fig. 4.13 and 4.14. The charge efficiency starts decreasing from 100%, when the battery state of charge reaches 75%. The point to be concluded here is, charging a battery

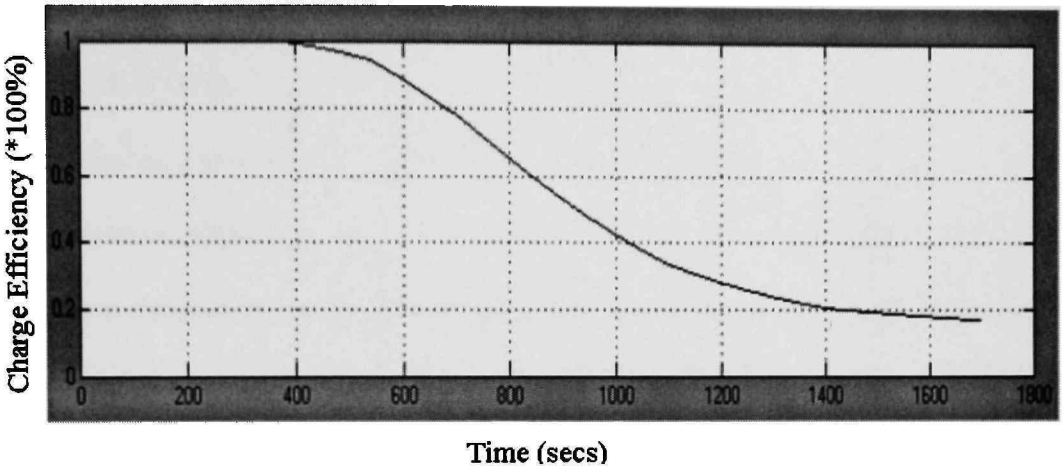

Fig. 4.14 Charge efficiency during charge

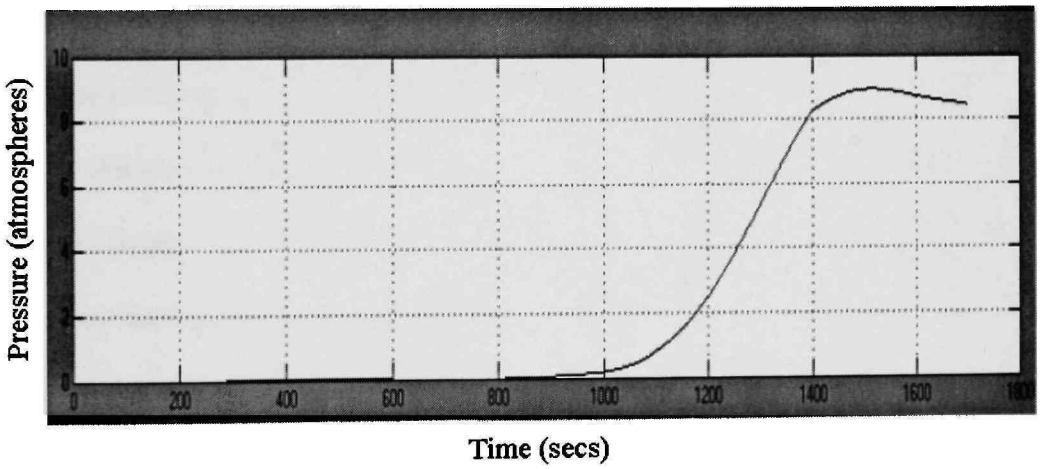

Fig. 4.15 Cell pressure variation during overcharge

at higher rates leads to high rate of oxygen generation. Fig. 4.15 plots the results of pressure profiles. It is assumed in this model that the oxygen gas is the only contributor to the battery pressure which occurs only during the overcharging of the batteries. Depending on the charge rate and the charge input of the battery, the pressure rise is

computed using the pressure block. However, the cell pressure increases substantially only after a certain point where the rate of oxygen generation at the nickel electrode begins to exceed the rate of oxygen recombination at the MH electrode [11]. This can be observed after 100% of charge input when charged at low rates. This onset of pressure build-up occurs earlier if the charge rates are higher which happened in this example. The battery pressure, which is initially 0 atmospheres, started to build up after 1000seconds of charge time. However, the percentage of charge input at this time is only 50%. But, since it is subjected to higher charge rates, the pressure starts increasing during the charge period and finally reaches 9 atmospheres during the overcharge period. Thereafter, if the battery is still charged the pressure vents break open resulting in adverse affects. It's therefore understood that oxygen generation during charging of the batteries leads to pressure build up as well as controls the charge at higher rates.

Another issue which comes into the picture during the overcharge periods is the battery temperature. The assumption made at this point is that the battery temperature increases during charge and overcharge periods and is ignored during discharge periods. Moreover the data used to model the empirical equation of battery temperature is restricted to charge rates ranging from 0.1C to 1C, beyond which the temperature curve follows an exponential relation and leads to high temperature profiles. Hence, the simulation results of the temperature and thermal runaway behavior of the batteries is observed using cycle 3 as the reference input in which the battery is subjected to a maximum charge rate of 1C.The input cycle 3 considered here is shown in Table 4.2.

Table 4.2 Input cycle 3

Time(sec)	0	300	1000	1500	5000	6400
Current(A)	0	0	8	12	19.5	13

Table 4.2 is shown in Fig. 4.16. Here the battery is charged to 120% of the rated capacity. Fig. 4.17 indicates the temperature profile. The fast charge rates serve to accentuate the slope changes. The battery temperature rises to 45^0C since it is charged at a rate of 1C.Inpractice a charge rate of 1C is recommended for restoring a discharged battery to full capacity. For charging schemes that then rely on a timed 'topping' charge to ensure complete charge, a rate of 0.1**C** appears to balance adequate charge input with minimum adverse effects in overcharge.

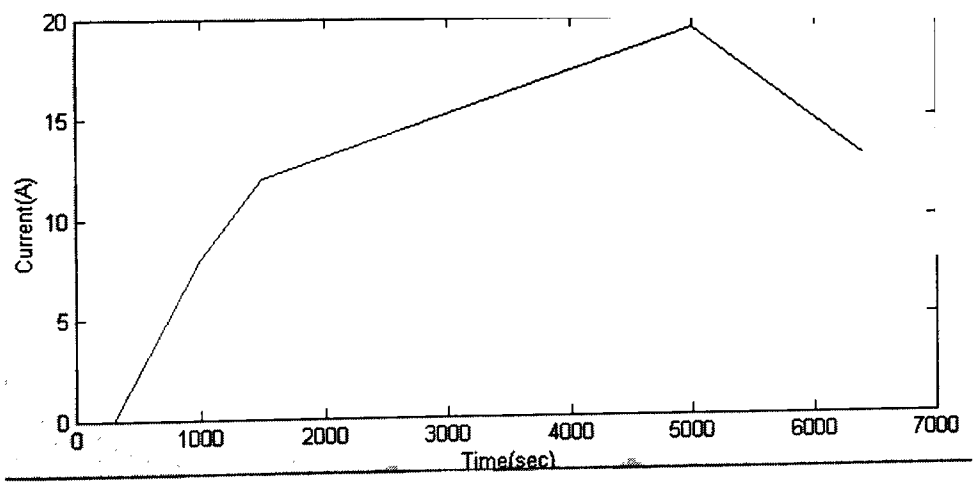

Fig. 4.16 Current input cycle 3

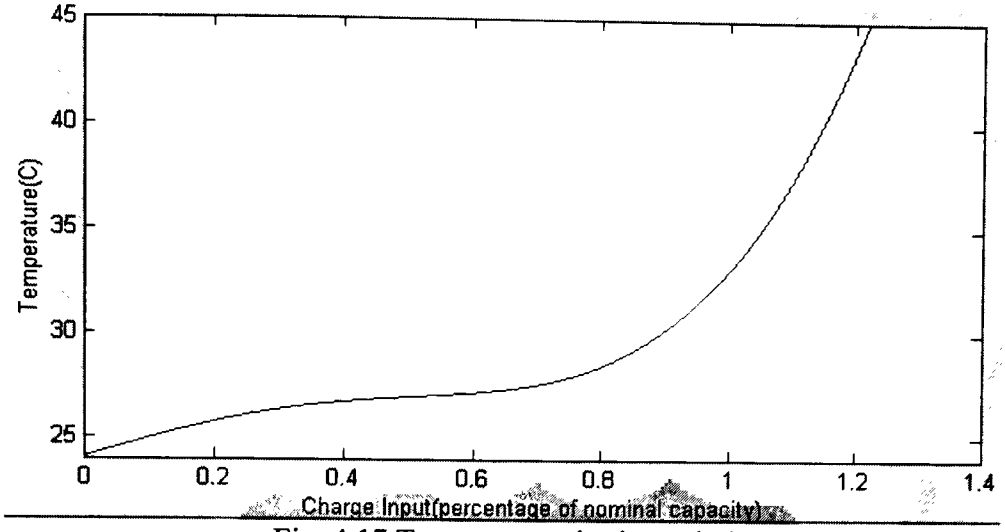

Fig. 4.17 Temperature rise in cycle 3

4.4 Validation of Results

The model developed is validated to some extent for a few parameters. Since there is no real test data available by which the model can be compared, PSAT is chosen to validate the model. It is modeled as a voltage source with a resistor in series. However, it is the most basic model (thevenin equivalent) .The resistor acts as a charging resistance during charge and discharging resistance during discharge. All the three parameters, V_{OC}, R_C (charging resistance) and R_D (discharging resistance) are just function of the state of charge. PSAT has the data for these parameters which uses them in truth tables with state of charge as the input. The results of this model, when subjected to charge and discharge in the vehicle are compared with the simulation results of the model in this thesis.

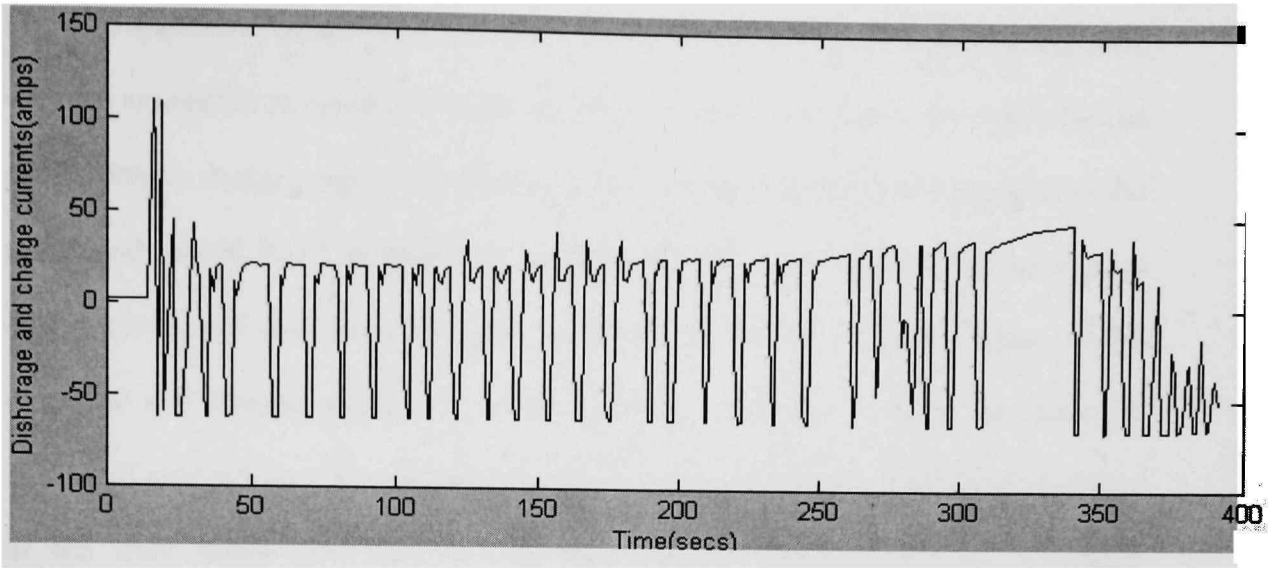

Fig. 4.18 Reference input cycle 1 under charge and discharge

However, this is restricted to state of charge and battery pack voltage. Fig. 4.18 is the reference cycle used as the input to the model developed and the PSAT model. The simulation result of the model follows the same pattern as PSAT model result shown in Fig. 4.19.

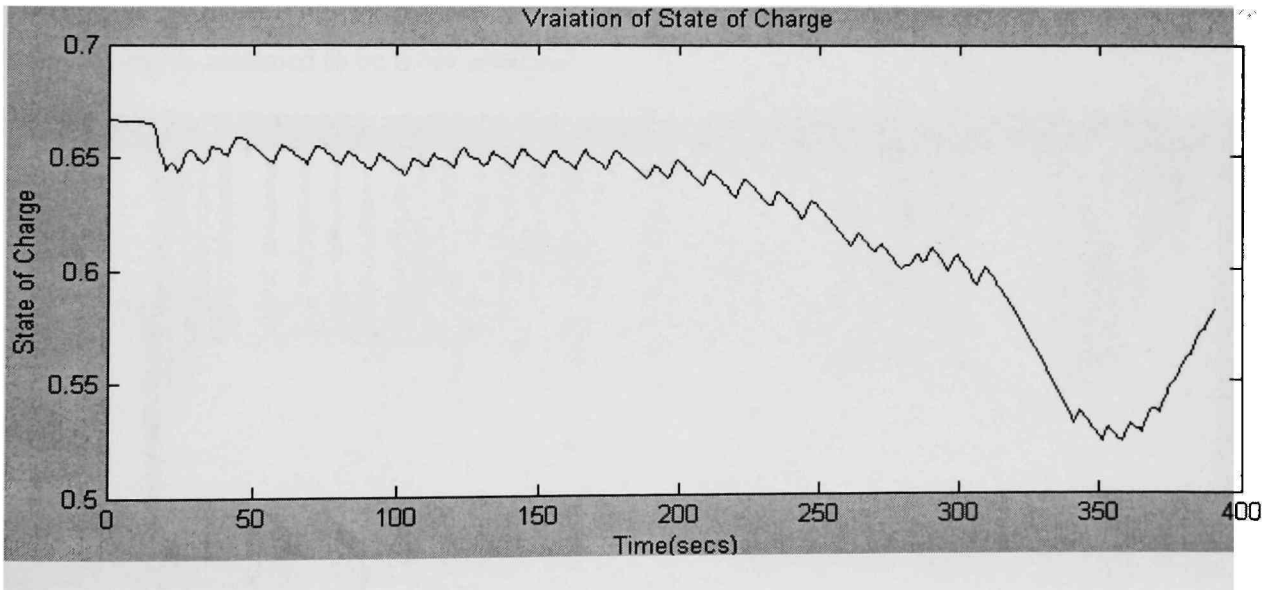

Fig. 4.19 State of charge

Fig. 4.20 shows the battery pack voltage of the PSAT model. This is in good comparison with the simulation result (Fig. 4.8) in the general shape of the curve. However, the end point voltages during peak power charge and discharges differed in the two models .As mentioned earlier, PSAT is used with limited data. The computation of battery voltage during the charge and discharge cycles is function of state of charge. Based on the discharge and charge currents, the state of charge algorithm in PSAT computes the amount of charge lost or gained and calculates the state of charge, which acts as the input to the truth tables for V_{OC}, R_C and R_D .The final voltage is then calculated using $E_O = V_{oc} - I \times R$, where 'I' is either charge or discharge current and R=R_C during charge and R_D during discharge. However, discharge and charge rate, which vary the mid point voltage and voltage peaks of the voltage profiles, are not considered in the PSAT model, due to which the end point and peak voltages vary for both the models. The model developed in this thesis incorporates the voltage profiles at various discharge and charge intervals and is assumed to be more accurate.

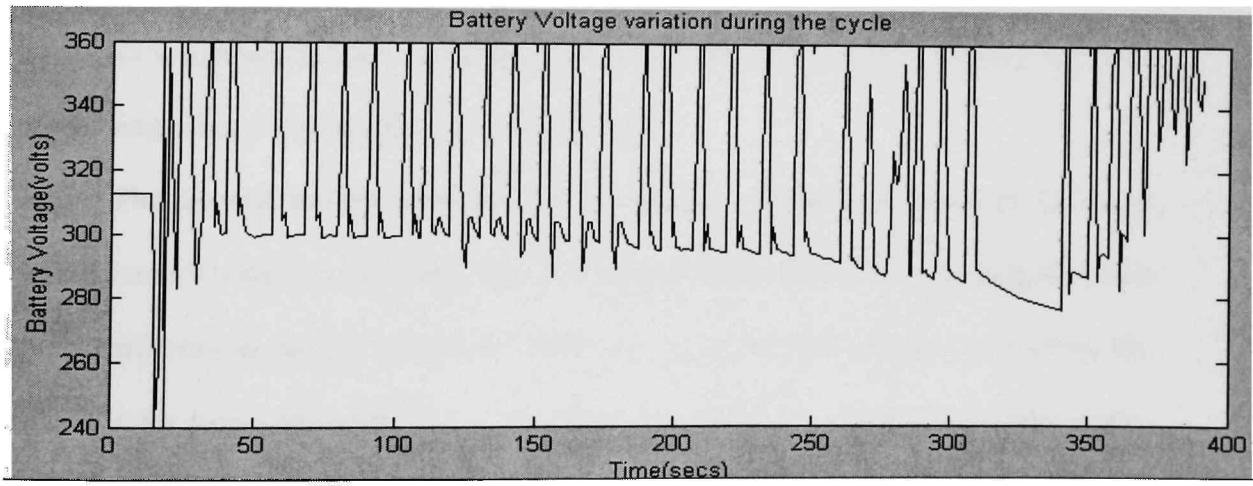

Fig. 4.20 Battery voltage

CHAPTER V

CONCLUSIONS

One way to improve the air quality in urban areas is to replace conventional IC engine automobiles with HEVs powered by rechargeable batteries. Batteries are an essential component of the HEVs under development. Simulation tools are essential in this aspect and enables battery design and improvement. Vehicle simulators are capable of dealing with various charge and discharge regimes. PSAT is an excellent simulation tool for vehicle analysis. Comparisons were made between the simulation results of the model with the PSAT for a high voltage NiMH battery pack. Good agreement was obtained between the two models in the shape of profile. However, there were differences in the magnitude due to several other variables coming into the picture for the model developed in this thesis. Simulations were performed to analyze the effects of oxygen reactions taking place in the batteries. However, the parameters of concern like charge efficiency and pressure have not been validated with any of the other models, since these issues are neglected in many of the standard simulation tools and are relatively new area of challenge and research in the design of batteries.

The battery model developed in this thesis is based on literature [11] and manufacturer's data [12, 13]. This data is processed using curve fitting packages to find the coefficients of several equations. However, since the data chosen to develop the model is for particular range, use of the input parameters like the discharge and charge rates beyond this data rage causes problems. One assumption made in the development the model is that battery temperature rises only during charge and does not have any

effect during the discharge. However, there is a minor change in the module temperature during discharge, but none of the manufacturer datasheets mention this heat dissipation behaviour during discharge. Since the model is based on the development of empirical equations rather than physical models, complete data is needed in the development of such models. Hence, this model can further be improved in two areas (1) extending the battery thermal model for not only charge but also during discharge; (2) extending the model to high charge and discharge rates of greater than 10C.

REFERENCES

1. Robert Kost, "DOE Hybrid Electric Vehicle Program . . . Why HEVs", Office of Transportation Technologies, from http://www.ott.doe.gov/pdfs/whyhev_factsheet.pdf, Washington, DC, 1999.

2. Philip Patterson, "Quantifying the Fuel Use and GHG Reduction Potential of EVs and HEVs." Retrieved April 26, 2002, from http://www.ott.doe.gov/pdfs/evs17.pdf

3. Rogelio A. Sullivan, "The technical background of Electric vehicles", Office of transportation technologies, from http://www.ott.doe.gov/pdfs/techhev_factsheet.pdf, Washington, DC, 1999

4. David Linden and Thomas .B Reddy, *Handbook of Batteries*, McGraw Hill, New York, 2002.

5. Dr.Raymond A. Sutula, "Energy Storage Technologies . . . for Hybrid Electric Vehicles", office of transportation technologies, from http://www.ott.doe.gov/pdfs/energyhev_factsheet.pdf, Washington, DC, 1999

6. H.L.Chan, D.Sutanto, "A New Battery Model for use with battery storage systems and electric vehicles power systems." Retrieved July 29, 2002, from Jonas Hellgren, Chalmers University of Technology, Gothenburg, Sweden.

7. ADVSIOR Documentation, "Energy Storage System." http://www.ctts.nrel.gov/analysis/advisor_doc/energy_storage.htm

8. Microsim Application Notes, "Using P-Spice to simulate discharge behavior of common batteries, MicroSim Corporation", Irvine, California, pp. 260-286,October 1996. Retrieved October 14, 2002, from http://kahuna.sdsu.edu/pspice/appnts.pdf

9. Thomas L.Martin "Balancing Batteries, Power, and Performance: System Issues in CPU Speed-Setting for Mobile Computing" Ph.D. Dissertation, Carnegie Mellon University, Pittsburgh, Pennsylvania, 1999. Retrieved May 25, 2002, from http://www.ece.vt.edu/~tlmartin/research/diss_final_3.pdf

10. Thermo Analytics Inc "Battery modeling" from http://www.thermoanalytics.com/support/publications/batterymodelsdoc.html

11. W.B.Gu, C.Y.Wang, S.M.Li, M.M.Geng, B.Y.Liaw, *Modeling discharge and charge characteristics of nickel-metal hydride batteries*, Electrochimica Acta, Pergamon, Oxford, pp. 4525-4541, 1999.

12. Discharge data sheet of HHR 650D Panasonic EV battery, Panasonic Inc.

13. NiMH application manual
www.data.energizer.com

14. Michael M.D.Ross, "A Simple but comprehensive Lead-Acid Battery Model for Hybrid System Simulation", GPCo, Inc., Varennes, Quebec. Retrieved October 23, 2002, from http://cetc-varennes.nrcan.gc.ca/eng/publication/2002-049e.pdf

15. Oakdale Engineering. DataFit 8.0 Trial Version. Curve fitting software for nonlinear regression [Computer software and manual]. Retrieved from http://www.curvefitting.com/download.htm#DataFit%20Downloads

16. Systat Software Inc. TableCurve 2D curve fitting software [Computer software and manual]. Retrieved from http://www.systat.com/products/TableCurve2D/

PERMISSION TO COPY

In presenting this thesis in partial fulfillment of the requirements for a master's degree at Texas Tech University or Texas Tech University Health Sciences Center, I agree that the Library and my major department shall make it freely available for research purposes. Permission to copy this thesis for scholarly purposes may be granted by the Director of the Library or my major professor. It is understood that any copying or publication of this thesis for financial gain shall not be allowed without my further written permission and that any user may be liable for copyright infringement.

Agree (Permission is granted.)

_____ _____

Student Signature Date

Disagree (Permission is not granted.)

_____ _____

Student Signature Date